PHYSICAL REVIEW D VOLUME 54, NUMBER 12 15 DECEMBER 1996

# Winding transitions at finite energy and temperature: An O(3) model

Salman Habib
*Theoretical Division, MS B288, Los Alamos National Laboratory, Los Alamos, New Mexico 87545*

Emil Mottola
*Theoretical Division, MS B285, Los Alamos National Laboratory, Los Alamos, New Mexico 87545*

Peter Tinyakov
*Institute for Nuclear Research of the Russian Academy of Sciences, 60th October Anniversary Prospect, 7a, Moscow 117312, Russia*
(Received 12 July 1996)

Winding number transitions in the two-dimensional softly broken O(3) nonlinear $\sigma$ model are studied at finite energy and temperature. New periodic instanton solutions which dominate the semiclassical transition amplitudes are found analytically at low energies, and numerically for all energies up to the sphaleron scale. The Euclidean period $\beta$ of these finite energy instantons *increases* with energy, contrary to the behavior found in the Abelian Higgs model or simple one-dimensional systems. This results in a *sharp crossover* from instanton-dominated tunneling to sphaleron-dominated thermal activation at a certain critical temperature. Since this behavior is traceable to the soft breaking of conformal invariance by the mass term in the $\sigma$ model, semiclassical winding number transition amplitudes in the electroweak theory in $3+1$ dimensions should exhibit a similar sharp crossover. We argue that this is indeed the case in the standard model for $M_H < 4M_W$. [S0556-2821(96)01324-0]

PACS number(s): 11.15.Kc, 11.10.Lm, 11.10.Wx, 12.15.−y

## I. INTRODUCTION

Gauge theories of the strong and electroweak interactions are characterized by a multiple vacuum structure. Tunneling transitions between different vacua are responsible for physically interesting effects, such as baryon-number violation in the electroweak theory [1]. At zero temperature and energy these winding number transitions are dominated by the familiar zero energy instanton solutions of the Euclidean field equations, with vacuum boundary conditions [2].

At finite temperatures thermal activation over the potential barrier separating the multiple vacua can take place, in addition to quantum tunneling. The static classical solution whose energy is equal to the top of this barrier between neighboring vacua is the sphaleron [3]. At sufficiently high temperatures, transitions between different winding number sectors are dominated not by quantum tunneling but by classical thermal activation, with a rate controlled by the energy of the sphaleron [4].

In simple one-dimensional quantum mechanics, as the temperature is increased, there is typically a smooth crossover from zero energy quantum tunneling via the instanton to high temperature thermal activation via the sphaleron [5]. The corresponding classical solutions which interpolate between these two situations are known as periodic instantons (or ''calorons'') [6,7]. These finite energy solutions of the classical Euler-Lagrange equations possess turning points at finite Euclidean time $\beta$, and dominate the semiclassical transition rate at a temperature related to the Euclidean period by $k_B T = \hbar/\beta$. (Hereafter, we set $\hbar = k_B = c = 1$, so that $T = \beta^{-1}$.)

Similar considerations are expected to apply to finite energy winding number transitions in quantum field theory, although there the situation is much less well explored and very few of the required Euclidean periodic classical solutions are known. In particular, it is not clear *a priori* if the smooth crossover of the transition rate from quantum tunneling to thermal activation is a generic feature, or if not, on what aspects of the field theory this behavior depends. Our purpose in this paper is to investigate this question by finding and studying the finite energy periodic instanton solutions in a specific model, the O(3) nonlinear $\sigma$ model in two dimensions, modified by a suitable conformal symmetry-breaking term. This model is chosen for the many features it shares in common with spontaneously broken gauge theories in four dimensions, and in particular, the standard model of electroweak interactions. In the $SU(2)\times U(1)$ electroweak theory the rate of baryon-number-violating winding transitions at high energies remains an open question, despite considerable efforts in recent years [8]. A detailed study of the solutions of the classical nonlinear field equations of the theory appears to offer the best hope of addressing this issue [9,10].

The O(3) $\sigma$ model possesses the advantage of being simple enough that the zero energy instanton, the finite energy sphaleron, and the spectrum of linearized fluctuations about each of these solutions are all known analytically. These analytic results are fixed markers in the classical solution space that can be used as launching points for a detailed numerical study of the finite energy periodic instanton solutions, and which provide useful nontrivial checks on the numerical methods. The numerical techniques developed in the context of the $\sigma$ model may be applied then with considerably more confidence to four-dimensional gauge theories such as the electroweak theory. The present work may be regarded as the first step in this program.

The chief result of our study of periodic instanton solutions in the softly broken O(3) $\sigma$ model is that the Euclidean

 

period $\beta$ of the finite energy instanton solutions *increases* with increasing energy: i.e.,

$$\frac{d\beta(E)}{dE} > 0 , \tag{1.1}$$

for all energies from zero up to the sphaleron. Since the Euclidean solution with period $\beta$ is associated with the winding number transition amplitude at temperature $T=\beta^{-1}$, one might expect that it should be $T$ which increases with energy, and not $\beta$. Indeed, in simpler models, such as the one-dimensional quantum pendulum or the two-dimensional Abelian Higgs model, the very *opposite* behavior to Eq. (1.1) is found. Our analytic and numerical study of periodic instanton solutions in the O(3) model will show that Eq. (1.1) holds all the way up to the sphaleron energy, where the periodic instantons merge with the sphaleron. Continuing further to energies $E > E_{\rm sph}$ results in the periodic instanton solutions moving off into the complex domain with still increasing real period.

As we shall see, the main physical consequence of this increase of period with energy is that there is a sharp crossover from instanton-dominated quantum tunneling to sphaleron-dominated thermal activation at a certain critical temperature (of the order of the mass in the model), rather than a smooth transition between the two. Since this feature is traceable to the conformal invariance of the unbroken O(3) model, the same sharp crossover from quantum tunneling to thermal activation should be expected in four-dimensional gauge theories where the conformal and spontaneous gauge symmetry breaking arises from the Higgs sector vacuum expectation value. Thus, the global picture which emerges from our study of the space of classical Euclidean solutions and their contribution to fixed energy and fixed temperature winding number transitions in the O(3) model should be directly applicable to the electroweak theory. We present evidence that this is indeed the case, at least for not too large Higgs self-coupling, i.e., for a Higgs boson mass $M_H < 4M_W$.

The structure of the paper is as follows. In the next section we discuss the general properties of periodic instanton solutions and their contribution to winding number transition rates at finite energy and temperature, in the context of a quantum mechanical model with only one degree of freedom, viz., the simple pendulum. In Sec. III we review the O(3) nonlinear $\sigma$ model both before and after introducing the explicit soft symmetry-breaking mass term. The mass term is necessary in order for a finite energy sphaleron solution to exist. In Sec. IV we consider finite energy instantons in the softly broken $\sigma$ model, employing analytic techniques at low energies where perturbation theory about the zero energy instantons of the unbroken model is applicable, and discussing the behavior of the periodic solutions near the sphaleron energy $E_{\rm sph}$. In Sec. V we describe our numerical techniques and present results for the finite energy instanton solutions smoothly interpolating between the two limits. We conclude in Sec. VI with a discussion of our results, and their implications for the analogous winding number transitions in the electroweak theory.

## II. PERIODIC INSTANTONS IN QUANTUM MECHANICS

At finite temperature the partition function for a quantum system may be expressed as a path integral over configurations with fixed Euclidean periodicity $\beta$:

$$Z(\beta) = \int_{q(0)=q(\beta)} [\mathcal{D}q] \exp(-S[q;\beta]), \tag{2.1}$$

where $S$ is the classical Euclidean action evaluated on the configuration over one period $\beta$. If there is a small coupling in the problem which can be scaled out of the action by $S = s/g^2$ and we consider the weak coupling limit $g^2 \to 0$, then the path integral is dominated by the extrema of the classical action, i.e., solutions of the classical Euclidean equations of motion obeying periodic boundary conditions.

Strictly speaking only stable solutions, i.e., local minima of the action, can contribute to the true equilibrium partition function at finite temperature. However, we are interested here in calculating the rate of real time winding number transitions at finite temperature or energy. In order to contribute to such a transition rate a classical solution should not be a strict minimum but rather a saddle point possessing *exactly one* negative mode direction. Analytic continuation of the semiclassical approximation to $Z(\beta)$ in this one negative mode direction leads to an imaginary part which may be interpreted as a real time transition rate [11]. A similar conclusion follows from an analytic extension of the path integral in Eq. (2.1) to complex-valued configurations [12].

In systems with only one degree of freedom it is straightforward to find the relevant periodic instanton solutions with a single negative mode direction by simple quadrature. Since the energy is an integral of the motion, we have simply to calculate

$$\beta(E) = \oint \frac{dq}{\sqrt{2V(q) - 2E}} \tag{2.2}$$

over the periodic trajectory with fixed energy $E$ beginning and ending at the same turning point of the potential $V(q)$. The Euclidean action corresponding to this periodic trajectory is

$$S(\beta) = \oint dq \sqrt{2V(q) - 2E(\beta)} , \tag{2.3}$$

where $E(\beta)$ is obtained by inverting Eq. (2.2).

In order to make the discussion definite let us consider the case of a simple pendulum with the classical periodic potential,

$$V(q) = \omega^2 (1 - \cos q). \tag{2.4}$$

The periodic local minima of this potential at $q = 2n\pi$ correspond to the periodic ground-state vacuum structure we find in non-Abelian gauge theories. The local maxima at $q = (2n+1)\pi$ are the static but unstable ''sphaleron'' solutions of this simple model with energy:

$$E_{\rm sph} = 2\omega^2. \tag{2.5}$$

In this case the ratio of the zero point energy $\omega/2$ of the harmonic potential in the vicinity of the minima to the height

of the potential barrier between minima, i.e., $\omega/2E_{\rm sph}=(4\omega)^{-1}$ is the parameter which must be small (in units of $\hbar=I=1$) in order to justify a semiclassical treatment of the quantum pendulum with moment of inertia $I$ about its pivot point.

At very low temperatures and energies the winding number transitions between neighboring minima at 0 and $2\pi$ are dominated by quantum tunneling with a rate of order $\exp(-2S_0)$ where $S_0$ is the classical action for the zero energy kink solution,

$$\cos\left(\frac{q_0(\tau)}{2}\right)=-\tanh(\omega\tau), \tag{2.6}$$

which interpolates between the two minima in infinite Euclidean time $\tau$. The antikink solution is obtained from Eq. (2.6) by time reversal $\tau\to-\tau$ and the periodic trajectory beginning and ending at the same vacuum is a widely separated kink-antikink pair with total action $2S_0=16\omega\gg1$, which implies that tunneling is exponentially suppressed at zero temperature or energy.

At the same time it is quite clear that this exponential suppression disappears at temperatures or energies comparable to $E_{\rm sph}$ when the pendulum can jump over the barrier between the neighboring minima by classical thermal activation. The semiclassical behavior of the transition rate at intermediate energies and temperatures is easily found analytically in the case of the pendulum since both of the integrals (2.2) and (2.3) may be expressed in terms of the complete elliptic integrals **K** and **E** as

$$\beta=\frac{4}{\omega}\mathbf{K}(k) \tag{2.7}$$

and

$$S=8\omega[2\mathbf{E}(k)-(1-k^2)\mathbf{K}(k)], \tag{2.8}$$

where $k$ is the modulus of the elliptic functions, related to the energy by

$$\frac{dS}{d\beta}=E=2\omega^2(1-k^2)\quad\text{or}\quad k=\sqrt{1-\frac{E}{2\omega^2}}. \tag{2.9}$$

The actual periodic instanton solution $q(\tau)$ with these properties may be expressed in terms of a Jacobian elliptic function sn with modulus $k$ by

$$\cos\left(\frac{q(\tau)}{2}\right)=-k\,\mathrm{sn}(\omega\tau,k)\to\begin{cases}-\tanh(\omega\tau), & E\to0,\\ 0, & E\to2\omega^2.\end{cases} \tag{2.10}$$

The corresponding behaviors of the Euclidean period and action in these limits are

$$E(\beta)=2\omega^2k'^2\to\begin{cases}0, & \beta\to\infty,\\ E_{\rm sph}, & \beta\to\beta_-,\end{cases} \tag{2.11}$$

and

$$S(\beta)\to\begin{cases}16\omega, & \beta\to\infty,\\ E_{\rm sph}/T_-, & \beta\to\beta_-,\end{cases} \tag{2.12}$$

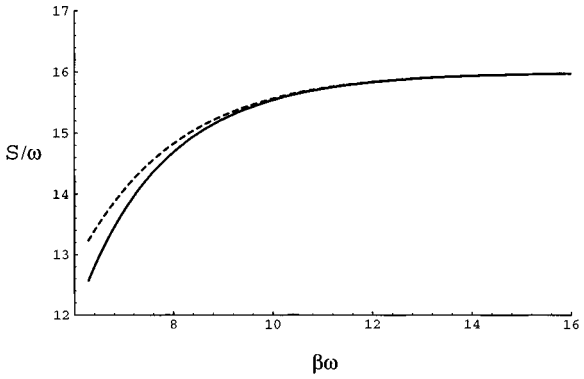


FIG. 1. Exact action, Eq. (2.8) (solid curve), and perturbative action, Eq. (2.26) (dashed curve) of the periodic instanton solutions of the simple pendulum model as a function of their Euclidean period $\beta$. The curves start at $\beta=\beta_-=2\pi/\omega$.

where

$$T_-\equiv\beta_-^{-1}=\frac{\omega}{2\pi} \tag{2.13}$$

and $k'\equiv\sqrt{1-k^2}$ is the complementary modulus of the elliptic functions.

In the first limit $E\to0$, we recover the vacuum-to-vacuum kink (or antikink) of Eq. (2.6) with periodicity $\beta\to\infty$, corresponding to a zero temperature winding transition of the pendulum by quantum tunneling. The second limit, $E\to E_{\rm sph}=2\omega^2$ and $\beta\to2\pi/\omega$ corresponds to thermal activation through the unstable, static sphaleron solution at $q=\pi$ halfway between the two neighboring periodic vacuum states. The action of the periodic instanton solution (2.10) interpolates smoothly between these two limits, as illustrated in Fig. 1.

Since $V''(q=\pi)=-\omega^2$ the eigenvalues of the second order fluctuation operator of the Euclidean action with periodic boundary conditions, expanded around the sphaleron solution, are

$$\lambda_n=\left(\frac{2\pi n}{\beta}\right)^2-\omega^2. \tag{2.14}$$

Hence, there is clearly exactly one negative mode corresponding to the unstable $n=0$ perturbation of the sphaleron solution in the high temperature regime $\beta<\beta_-$, where $\beta_-$ is just the period of the harmonic oscillation about the inverted potential $-V(q)$ at $q=\pi$. Thermal activation through the sphaleron dominates the transition rate for high temperatures $T>T_-$.

For $\beta>\beta_-$, i.e., low temperatures $T<T_-$, the sphaleron has more than one negative mode and does not dominate the semiclassical winding number transition rate. However, in this low temperature range the periodic instanton given by Eq. (2.10) possesses exactly one negative mode by the following standard argument. Since the periodic instanton obeys the classical Euclidean Euler-Lagrange equation,

$$\frac{d^2q}{d\tau^2}=V'(q), \tag{2.15}$$

it follows by differentiation that its time derivative is a zero mode of the second order fluctuation operator: i.e.,

$$\left(-\frac{d^2}{d\tau^2}+V''(q)\right)\dot{q}=0\,. \tag{2.16}$$

From the periodic behavior of $q(\tau)$ it follows that $\dot{q}$ has exactly one node in the interval $(0,\beta)$, and hence by a standard theorem of second order linear differential operators, the fluctuation operator,

$$-\frac{d^2}{d\tau^2}+V''(q)=-\frac{d^2}{d\tau^2}+2\omega^2k^2\mathrm{sn}^2(\omega\tau,k)-\omega^2 \tag{2.17}$$

must possess exactly one mode with no nodes and a lower (i.e., negative) eigenvalue. Hence, the finite energy periodic instanton solution (2.10) dominates the winding number transition rate for temperatures $T<\omega/2\pi$ and energies $E<2\omega^2$.

The one negative mode may be understood intuitively as the result of the attractive interaction between a kink and antikink which binds the pair into a kink-antikink ''molecule'' and lowers the classical action of the bound periodic instanton configuration. This attractive interaction may be studied analytically in perturbation theory at low energies. Since the same approach proves quite useful in more complicated models let us review the general method in the pendulum problem.

Since the kink solution $q_0(\tau)$ of Eq. (2.6) has zero energy we expect the periodic solution for small but finite energy to consist of an infinite chain of widely separated alternating kinks and antikinks which are very loosely bound. Thus, we consider the trial configuration

$$q(\tau)=\begin{cases} q_0(\tau), & 0\leqslant\tau\leqslant\beta/4,\\ q_0\left(\dfrac{\beta}{2}-\tau\right), & \beta/4\leqslant\tau\leqslant3\beta/4,\\ q_0(\tau-\beta), & 3\beta/4\leqslant\tau\leqslant\beta,\end{cases} \tag{2.18}$$

defined on the fundamental interval $[0,\beta]$, and consisting of a kink at 0 and $\beta$ and an antikink halfway between at $\beta/2$. This configuration may be repeated indefinitely along the $\tau$ axis to form an infinite chain of alternating kinks and antikinks. The configuration is everywhere continuous and has finite action per period,

$$\begin{aligned} S[q(\tau)]&=\int_0^\beta d\tau\left[\frac{1}{2}\dot{q}^2+V(q)\right]\\ &=4\omega^2\left[\int_{-\beta/4}^{\beta/4}d\tau\,\mathrm{sech}^2\omega\tau\right.\\ &\quad\left.+\int_{\beta/4}^{3\beta/4}d\tau\,\mathrm{sech}^2\omega\left(\frac{\beta}{2}-\tau\right)\right]\\ &=16\omega\tanh\left(\frac{\omega\beta}{4}\right)\\ &=16\omega-32\omega e^{-\omega\beta/2}+O(e^{-\omega\beta}), \end{aligned} \tag{2.19}$$

where we retain only the leading $\beta$ dependence for large $\beta$.

The configuration (2.18) is also a solution of the Euclidean equation (2.15) except at the matching points, $\tau=\beta/4$ and $\tau=3\beta/4$, where the first derivative is discontinuous. That is,

$$\begin{aligned} L[q(\tau)]&\equiv-\frac{d^2}{d\tau^2}q+V'(q)\\ &=-2\,\delta\left(\tau-\frac{\beta}{4}\right)\dot{q}_0\left(\frac{\beta}{4}\right)+2\,\delta\left(\tau-\frac{3\beta}{4}\right)\dot{q}_0\left(-\frac{\beta}{4}\right)\\ &=4\omega\,\mathrm{sech}\left(\frac{\omega\beta}{4}\right)\left[-\delta\left(\tau-\frac{\beta}{4}\right)+\delta\left(\tau-\frac{3\beta}{4}\right)\right]. \end{aligned} \tag{2.20}$$

These delta functions act as point sources for the field $q(\tau)$. If we expand about the trial configuration (2.18), $q\to q+\xi$, then the nonzero result of Eq. (2.20) implies that there are linear source terms for the fluctuations $\xi$. The effect of these sources on the action functional may be found by shifting the fluctuation

$$\xi(\tau)\to\xi(\tau)-\int_0^\beta d\tau'\,G_\beta(\tau,\tau')L[q(\tau')] \tag{2.21}$$

to remove the linear term [12,13]. The periodic Green's function $G_\beta(\tau,\tau')$ obeys

$$\begin{aligned} \left[-\frac{d^2}{d\tau^2}+V''(q)\right]G_\beta(\tau,\tau')&=\delta_\beta(\tau-\tau')\\ &=\frac{1}{\beta}\sum_{n=-\infty}^{\infty}\exp[2\pi i(\tau-\tau')n/\beta]. \end{aligned} \tag{2.22}$$

To leading order in the exponentially small tail $e^{-\omega\beta/2}$ we can replace $V''(q)$ by its vacuum value $\omega^2$ and use the free (perturbative) periodic Green's function,

$$G_\beta(\tau,\tau')=\frac{1}{2\omega}\frac{1}{\sinh(\beta\omega/2)}\cosh\omega\left(|\tau-\tau'|-\frac{\beta}{2}\right), \tag{2.23}$$

for $\tau$ and $\tau'$ in the fundamental interval $[0,\beta]$.

To leading order in $L[q]$ the effect of the shift (2.21) to remove the linear term is to alter the action at quadratic order: i.e.,

$$\begin{aligned} S[q(\tau)]\to S[q(\tau)]&\\ -\frac{1}{2}\int_0^\beta d\tau\int_0^\beta d\tau'\,L[q(\tau)]G_\beta(\tau,\tau')L[q(\tau')]&. \end{aligned} \tag{2.24}$$

Substituting Eqs. (2.20) and (2.23) into this extra term leads to the result that the action of the periodic instanton is the action of the trial kink-antikink configuration (2.19) shifted by

$$-8\omega^2\mathrm{sech}^2\left(\frac{\omega\beta}{4}\right)\left[G_\beta\left(\frac{\beta}{4},\frac{\beta}{4}\right)+G_\beta\left(\frac{3\beta}{4},\frac{3\beta}{4}\right)-G_\beta\left(\frac{\beta}{4},\frac{3\beta}{4}\right)-G_\beta\left(\frac{3\beta}{4},\frac{\beta}{4}\right)\right]=-32\omega e^{-\omega\beta/2}+O(e^{-\omega\beta}). \quad (2.25)$$

Adding this shift to Eq. (2.19) we find that the action of the periodic instanton in the pendulum model is

$$S(\beta)=16\omega-64\,\omega e^{-\omega\beta/2}+O(e^{-\omega\beta}), \quad (2.26)$$

while its energy becomes

$$E(\beta)=\frac{dS}{d\beta}=32\omega^2 e^{-\omega\beta/2}+O(e^{-\omega\beta}) \quad (2.27)$$

to leading order in the expansion in powers of $E/E_{\rm sph}=16\exp(-\omega\beta/2)$. The negative second term in Eq. (2.26) is the effect of the short-ranged attractive interaction between neighboring kinks and antikinks along the chain that lowers the action functional to first order in the two-body interaction $\exp[-\omega(|\tau_1-\tau_2|)]$ between them.

This result and this general method of patching together zero energy kinks and antikinks can be checked in the pendulum example by comparison to the exact results (2.7)–(2.9) in terms of the elliptic functions. Indeed, in the low energy limit the modulus $k\to 1$ and the expansion of the complete elliptic integrals in powers of the complementary modulus,

$$k'\equiv\sqrt{1-k^2}\to 4\,e^{-\omega\beta/4}, \quad (2.28)$$

yields

$$S(\beta)=16\,\omega\left(1-\frac{k'^2}{4}+O(k'^4)\right)=16\,\omega-64\,\omega e^{-\omega\beta/2}+O(e^{-\omega\beta}) \quad (2.29)$$

and

$$E(\beta)=2\omega^2 k'^2=32\,\omega^2 e^{-\omega\beta/2}+O(e^{-\omega\beta}), \quad (2.30)$$

which coincides with Eqs. (2.26) and (2.27). The exact and perturbative results for the action as a function of $\beta$ are compared in Fig. 1.

As $\beta$ is decreased from infinity to $\beta_-$ and $E$ is increased from zero to $E_{\rm sph}$, the kink-antikink molecule becomes more tightly bound and the nonlinear interactions between the kink and antikink become more important. The action of the periodic instanton (2.10) decreases from $2S_0=16\omega$ to $S(\beta_-)=E_{\rm sph}\beta_-=4\pi\omega<2S_0$ and it is easy to see from the properties of the elliptic functions involved that the derivative $d\beta(E)/dE$ is *negative* everywhere in the interval $(0,E_{\rm sph})$. At $E=E_{\rm sph}$, $\beta=\beta_-$, $S=E_{\rm sph}\beta_-$, and the periodic instanton solution (2.10) becomes *identical* to the sphaleron. Beyond this point we no longer have a real periodic instanton solution. This presents no difficulty as analytic continuation of the solution (2.10) for $E>E_{\rm sph}$ is easily accomplished by allowing the modulus $k$ to become purely imaginary. Then, the solution $q(\tau)$ becomes complex (in fact, $\pi$ plus a purely imaginary function of $\tau$), but the period (2.7) and action (2.8) remain real and continue to decrease as the energy is increased. However, the fluctuation operator (2.17) now has additional negative modes and hence the analytically continued solution no longer dominates the winding number transition rate, its place having been taken by the static sphaleron for $T>\omega/2\pi$. At $\beta=0.61627\beta_-$ and $E=5.74914E_{\rm sph}$, the action (2.8) of the complex instanton actually plunges through zero and then becomes negative, finally going to $-\infty$ as $E\to\infty$ and $\beta\to 0$. The situation is most conveniently illustrated graphically in Fig. 2. Notice that, in this simple pendulum model the zero temperature tunneling exponent $2S_0$ is equal to the thermal activation Boltzmann exponent $E_{\rm sph}/T$ at $T=\omega/8$ which is *less than* $T_-=\omega/2\pi$.

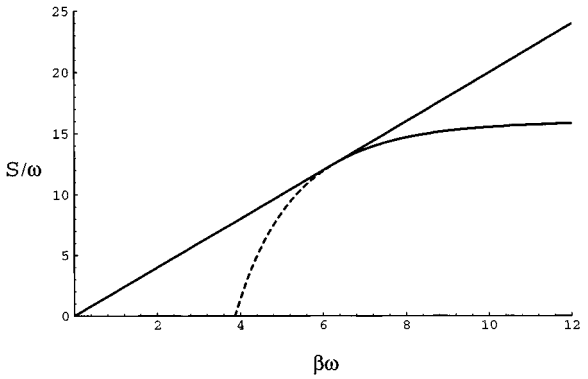


FIG. 2. The action of the periodic instanton and sphaleron as a function of $\beta$ for the simple pendulum model. The instanton solution goes from real (solid curve) to complex (dashed curve) at $\beta=\beta_-$, where the sphaleron action $S=E_{\rm sph}\beta$ (straight line) is tangent to the curve. At $\beta=\beta_{\rm cr}=8/\omega>\beta_-$ the zero energy instanton action $2S_0$ equals the sphaleron action.

The merging and resplitting off into the complex domain of the periodic instanton solution as $\beta$ is decreased through $\beta_-$ is an interesting aspect of the behavior we have just sketched. This may be understood from the fact that near $\beta=\beta_-$ the eigenvalues of the static sphaleron fluctuation operator $\lambda_{\pm 1}$ in Eq. (2.14), go through zero. Whenever a zero mode appears in the second order fluctuation operator this indicates the existence of a nearby solution of the classical equations. When the zero mode is not related to a symmetry of the action but instead appears only at special values of a parameter in the boundary conditions, then the solution generally splits off or *bifurcates* into two (or more) different solutions as the parameter is varied. Conversely, as the parameter is varied in the opposite direction two or more solutions *merge* at the critical value of the parameter. This is just the case for the static sphaleron solution as the parameter $\beta$ is varied through $\beta_-$. At $\beta_-$ we find another classical solution with the same Euclidean period splitting off or merging with the static sphaleron in the (generally complex) direction of the zero mode in function space. Hence, near $\beta=\beta_-$ the periodic instanton solution is given approximately by a small perturbation of the sphaleron in the relevant zero mode direction, viz.,

$$q(\tau)\simeq q_{\rm sph}+\delta\cos(\omega\tau+\phi), \quad (2.31)$$

where $\phi$ is an arbitrary phase of the periodic solution and $\delta$ is a small parameter that goes to zero as $\beta\to\beta_-$. The

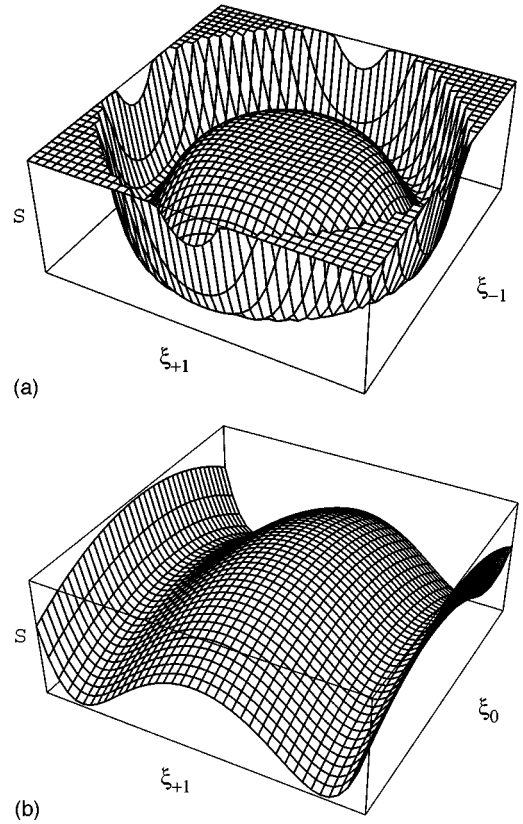


FIG. 3. The action $S$ as a function of the variables $\xi_{\pm 1}$ (a) corresponding to the two near-zero mode directions, and as a function of one of these variables and the negative mode direction $\xi_0$, (b) for fixed $\beta$ slightly larger than $\beta_-$. The ring of extrema of $S$ in the first figure [due to the arbitrary phase in Eq. (2.31)] or the two outer extrema in the second figure correspond to the periodic instanton solution. As $\beta$ approaches $\beta_-$ these extrema merge with the sphaleron in the center. Since the periodic instanton solution has one negative mode and lower action than that of the sphaleron, it dominates the winding number transition rate which is controlled by the lowest available saddle in (b).

arbitary phase informs us that in fact there is a one parameter U(1) family of periodic instanton solutions which merge and then resplit off from the sphaleron at $\beta_-$ which accounts for the two zero mode directions, $n=\pm 1$ at $\beta=\beta_-$.

This situation is also easier to visualize graphically. Let us suppress all but the relevant zero mode directions and represent the action functional $S$ as a function only of a few variables $\xi_i$ together with the parameter $\beta$. Clearly, as $\beta$ varies the surfaces of $S=\text{const}$ change, as does the location of the extrema, $\partial S/\partial \xi_i = 0$. At certain values of $\beta$ if two of the extrema split off or merge, there is a zero eigenvector of the second order fluctuation matrix $\partial^2 S/\partial \xi_i \partial \xi_j$. Since the number of extrema is determined by the global properties of $S$, generally the bifurcation of extrema does not mean that their total number changes discontinuously, but rather that real extrema move into the complex domain as the parameter $\beta$ is varied through $\beta_-$. The U(1) invariance of the action under the arbitrary phase $\phi$ implies that a ring of equal action extrema converges on the sphaleron and then becomes complex for $\beta<\beta_-$. This action as a function of the three relevant variables $\xi_{\pm 1}$ and $\xi_0$ is illustrated in Fig. 3.

To summarize this discussion, the physical interpretation of the properties of the classical Euclidean periodic solutions for winding number transitions in the simple pendulum model is clear. At low temperatures $T<1/\beta_-$, the periodic instanton solution dominates the vacuum-to-vacuum winding number transition amplitude which is exponentially suppressed. As the temperature is raised the classical periodic solutions become a more closely spaced chain of kinks and antikinks with a larger nonlinear interaction between them that lowers the action. The tunneling rate becomes less suppressed as the turning points of the periodic solution move inwards toward their midpoint at $q=\pi$, corresponding to less quantum tunneling and more thermal motion in the allowed region. At $T=T_-=\omega/2\pi$, the turning points become identical with the sphaleron at $q=\pi$ and tunneling has been replaced by purely classical thermal activation which is still only slightly less exponentially suppressed than the zero temperature transition rate. At this and all higher temperatures the winding number transition rate is dominated by the sphaleron which has exactly one negative mode for $T>T_-$. The periodic instanton solution moves off into the complex domain and no longer contributes to the transition rate, which becomes less and less exponentially suppressed as the temperature is raised further. Finally, at temperatures greater than of order $E_{\text{sph}}=2\omega^2$, the exponential suppression disappears entirely and the pendulum swings freely around its pivot, the probability of finding the pendulum anywhere then becoming nearly uniform as the temperature is raised still further.

This fixed temperature discussion has a natural analogue at fixed energy. The probability of making a winding number transition at fixed energy between $E$ and $E+dE$ may be expressed in the form,

$$P(E)dE=\sum_{i,f} |\langle f|\mathcal{S}\mathcal{P}_E|i\rangle|^2, \tag{2.32}$$

where $\mathcal{S}$ is the $\mathcal{S}$ matrix, $\mathcal{P}_E$ is a projector onto energy $E$, and the initial and final states $|i\rangle$ and $|f\rangle$ lie in different winding sectors in the energy interval $E$ to $E+dE$. Periodic instantons appear again as the configurations which saturate $P(E)$, and the probability is given, with exponential accuracy, by the exact analogue of the quantum-mechanical formula [5,7]

$$P(E)dE\sim\exp[-W(E)]dE, \tag{2.33}$$

where

$$W(E)=S[\beta(E)]-E\beta(E) \tag{2.34}$$

is the Legendre transform of $S(\beta)$. The relevant instanton solutions should be considered now as fixed in energy rather than in periodicity $\beta$.

The initial and final multiparticle states can be read off from the analytic continuation of the finite energy periodic instanton into Minkowski time at its turning points. Hence, periodic instanton solutions to the classical Euclidean equations contain nontrivial information about multiparticle transition amplitudes between different winding number sectors at finite energy. It has been suggested that by suitably modifying the boundary conditions in the complex time plane,

information about transition amplitudes from few particle initial states to many particle final states may be obtained as well [10].

The fixed temperature transition rate can be reconstructed from the fixed energy tunneling probability by weighting with a Boltzmann distribution and integrating over energy. To exponential accuracy we have

$$\Gamma(T)=\int_0^\infty dE\exp\left(-\frac{E}{T}\right)P(E)\sim\int_0^\infty dE\exp\left(-\frac{E}{T}-W(E)\right). \tag{2.35}$$

Evaluating this integral by the method of steepest descent (which is valid in the limit of arbitrarily weak coupling $\omega^{-1}\sim g^2\to 0$, provided $T$ is coupling independent) gives the saddle-point condition,

$$\frac{1}{T}=-\frac{dW}{dE}=\beta(E), \tag{2.36}$$

by the properties of the Legendre transform $W=S-E\beta$. Hence, we recover the connection between the temperature and Euclidean periodicity of the instanton solution in this way. Evaluating the second derivative of the exponent in Eq. (2.35) at this saddle point yields

$$-\frac{d^2W}{dE^2}=+\frac{d\beta(E)}{dE}, \tag{2.37}$$

which tells us that only solutions for which the quantity in Eq. (2.37) is *negative* can contribute to the fixed temperature rate $\Gamma(T)$. On the other hand, classical solutions for which this derivative is positive cannot contribute to the integral (2.35) since they are local *minima* rather than maxima of the the exponent in the integrand. In the case of the simple quantum pendulum example considered in detail in this section Eq. (2.37) is indeed negative and the periodic instantons given by Eq. (2.10) do contribute to the finite temperature transition rate $\Gamma(T)$ in the expected way, for all temperatures $T\leqslant T_-$. We turn now to the O(3) $\sigma$ model where the behavior of the periodic instanton solutions, the corresponding quantity (2.37) and the crossover from quantum tunneling to thermal activation, are all quite different.

## III. THE O(3) $\sigma$ MODEL

The two-dimensional O(3) nonlinear $\sigma$ model is defined by the Euclidean action functional,

$$S=\frac{1}{2g^2}\int dx d\tau(\partial_\mu n^a)^2, \tag{3.1}$$

where $n^a(x)$, $a=1,2,3$ are three components of a unit vector, $n^a n^a=1$, and $\mu=\tau,x$. The constraint on the magnitude of $n^a$ at every spacetime point is the source of nonlinearity in the model. A convenient parametrization in which the constraint is removed at the price of explicit nonlinearity is the complex field definition,

$$w\equiv\frac{n_1+in_2}{1-n_3}. \tag{3.2}$$

Introducing the complex coordinate,

$$z\equiv x+i\tau\equiv re^{i\theta}, \tag{3.3}$$

in terms of the spatial position $x$ and Euclidean time $\tau$ enables us to rewrite the action (3.1) in the equivalent forms

$$S=\frac{2}{g^2}\int dx d\tau\frac{\partial_\mu w\partial_\mu\overline{w}}{(1+\overline{w}w)^2}$$

or

$$S=\frac{4}{g^2}\int dx d\tau\frac{1}{(1+\overline{w}w)^2}\left(\frac{\partial w}{\partial z}\frac{\partial\overline{w}}{\partial\overline{z}}+\frac{\partial\overline{w}}{\partial z}\frac{\partial w}{\partial\overline{z}}\right), \tag{3.4}$$

where the overbar denotes complex conjugation and $\overline{w}=\overline{w(z,\overline{z})}=w(\overline{z},z)$.

This model possesses some remarkable similarities with pure gauge theories in four dimensions. The most important properties which concern us here are the conformal invariance of the classical action $S$, and the existence of a periodic vacuum structure in the model. In connection with the conformal invariance we observe that the coupling constant $g$ is dimensionless and there is no length scale in $S$. Correspondingly, the quantum theory is logarithmically renormalizable and in fact, asymptotically free in the coupling $g$ [14].

The periodic structure should be clear from the fact that an O(3) rotation by $2\pi$ around any axis brings the vector $n^a$ back to itself. The topological winding number associated with this field periodicity will be made explicit if we identify the points at infinity of the complex plane in the coordinate $z=x+i\tau$. Then the plane has the topology of the sphere $S^2$. Since the field $n^a$ is also constrained to lie on $S^2$, the $n^a$ field is a map from $S^2$ to $S^2$ which is characterized by an integer winding number, given explicitly by

$$\begin{aligned}Q&=\frac{1}{8\pi}\int dx d\tau\epsilon^{\mu\nu}\epsilon_{abc}n^a\partial_\mu n^b\partial_\nu n^c\\&=\frac{1}{\pi}\int dx d\tau\frac{1}{(1+\overline{w}w)^2}\left(\frac{\partial w}{\partial z}\frac{\partial\overline{w}}{\partial\overline{z}}-\frac{\partial\overline{w}}{\partial z}\frac{\partial w}{\partial\overline{z}}\right).\end{aligned} \tag{3.5}$$

Comparing the latter form of the topological winding number with the action (3.4), it is clear that the action in any integer $Q$ topological sector is bounded from below, i.e.,

$$S\geqslant\frac{4\pi}{g^2}|Q| \tag{3.6}$$

and, moreover, that this bound is saturated by meromorphic functions $w$ of the complex variable $z$ or $\overline{z}$ [15]. In particular, the conformal map of $S^2$ to $S^2$, topologically equivalent to the identity map is the one instanton solution of the Euclidean equations with $Q=1$. This solution can be written in the form

$$w_0(z)=\frac{\rho}{z}=\frac{\rho}{r}e^{-i\theta}, \tag{3.7}$$

and has action

$$S_0=\frac{4\pi}{g^2}. \tag{3.8}$$

The anti-instanton solution is obtained from Eq. (3.7) by Euclidean time reversal which in the $w$ description is equivalent to complex conjugation.

The instanton and anti-instanton solution have zero Euclidean energy,

$$E_0=\frac{1}{2g^2}\int dx(-\partial_\tau n^a\partial_\tau n^a+\partial_x n^a\partial_x n^a)=0\,. \tag{3.9}$$

They correspond, respectively, to the classical Euclidean path of least action and its time reverse, connecting periodic vacua separated by unit winding number. Together, the instanton and anti-instanton constitute a periodic trajectory beginning and ending at the same vacuum state, with one negative mode corresponding to the attractive interaction between them, just as in the simple pendulum model. Hence, in the limit of weak coupling $g^2\to 0$ the rate for a unit winding number vacuum-to-vacuum tunneling transition is $\exp(-2S_0)=\exp(-8\pi/g^2)$ to exponential accuracy, and is strongly suppressed.

Because of the conformal invariance of the action (3.1), the zero energy instanton can have arbitrary scale $\rho$. This implies that the potential energy barrier between winding number sectors, i.e., the second term of Eq. (3.9) evaluated at $\tau=0$, which is proportional to $\rho^{-1}$, can be made arbitrarily small and no finite energy sphaleron solution exists in the symmetric O(3) model. This feature is quite different from the simple pendulum and Abelian Higgs models but is shared by the pure Yang-Mills theory in four dimensions.

In the electroweak theory conformal invariance is broken in the Higgs sector which then makes possible the existence of a classical sphaleron solution. In the O(3) $\sigma$ model the conformal invariance may be broken by adding to the action (3.1) the explicit mass term

$$S_m=\frac{m^2}{g^2}\int dx\,d\tau(1+n_3), \tag{3.10}$$

which also violates the O(3) symmetry and fixes the vacuum state to be $n^a_{(\mathrm{vac})}=(0,0,-1)$. In the Heisenberg spin language this corresponds to placing the system in an external magnetic field which aligns all the spins in the direction $n^a_{(\mathrm{vac})}$ at zero temperature.

When the $\sigma$ model has been modified in this way by the introduction of the soft symmetry-breaking mass term $S_m$,

$$S\to S+S_m\,, \tag{3.11}$$

the instanton configuration with arbitrary nonzero $\rho$ in Eq. (3.7) ceases to be an exact solution of the field equations, but there is now an exact sphaleron solution [16,17], namely,

$$n^1_{(\mathrm{sph})}(x)=-2\tanh(mx)\,\mathrm{sech}(mx),\quad n^2_{(\mathrm{sph})}(x)=0\,,$$

$$n^3_{(\mathrm{sph})}(x)=-1+2\,\mathrm{sech}^2(mx), \tag{3.12}$$

with finite energy,

$$E_{\mathrm{sph}}=\frac{8m}{g^2}. \tag{3.13}$$

Geometrically, this solution maps the infinite spatial line onto a great circle beginning and ending at the south pole, $n^3_{(\mathrm{vac})}=-1$. The sphaleron lies exactly halfway between the vacua of winding numbers 0 and 1, and $E_{\mathrm{sph}}$ is, therefore, the height of the potential energy barrier between these vacuum states, which is now fixed and finite.

Let us recall that the spectrum of time-independent perturbations around the static sphaleron has exactly one normalizable negative mode with the eigenfunction $u^a_-(x)=(0,\mathrm{sech}^2(mx),0)$ and the eigenvalue $\epsilon^2_-=-3m^2$. There are two zero modes of the spatial fluctuation operator corresponding to spatial translations of the sphaleron position and rotation of its great circle trajectory around the $n^3$ axis. The remaining eigenvalues are strictly positive and form a continuous spectrum with $\epsilon^2_+\geqslant m^2$. Taking the periodic $\tau$ dependence of the fluctuations into account yields the following eigenvalues for the full second order fluctuation operator of the action around the sphaleron solution:

$$\lambda_{n,\epsilon}=\left(\frac{2\pi n}{\beta}\right)^2+\epsilon^2. \tag{3.14}$$

Periodic boundary conditions are the appropriate ones for contributions to the path integral at finite temperature $T=\beta^{-1}$. By the same argument as in the one-dimensional pendulum the existence of one and only one negative eigenvalue (3.14), namely, $n=0$ and $\epsilon^2=\epsilon^2_-=-3m^2$ for $\beta<\beta_-\equiv 2\pi/|\epsilon_-|=2\pi/(\sqrt{3}m)=3.628m^{-1}$ implies that the sphaleron configuration contributes to the winding number transition rate for temperatures $T>T_-$. The sphaleron contribution to the rate per unit one-dimensional spatial volume can be expressed in the notation of the present paper in the form [16]

$$\Gamma_{\mathrm{sph}}=\frac{2}{\pi g^2}\,\frac{mT}{\sin(|\epsilon_-|/2T)}\exp[-E_{\mathrm{sph}}/T-h(m/T)], \tag{3.15}$$

where

$$h(m/T)\equiv-\frac{4m}{\pi}\int_0^\infty dk\left[\frac{1}{\omega_k^2}+\frac{1}{\omega_k^2+3m^2}\right]\ln(1-e^{-\omega_k/T}), \tag{3.16}$$

and

$$\omega_k\equiv\sqrt{k^2+m^2}. \tag{3.17}$$

The asymptotic form of this function in the high temperature limit $m\beta\ll 1$ is

$$h(m/T)\to-3\ln(m/T)-\frac{4m}{\pi T}\ln(m/T)-C+O(m/T), \tag{3.18}$$

where we take this opportunity to correct an error in the numerical evaluation of the constant $C$ in Eq. (5.7) of Ref. [16], viz. [18],

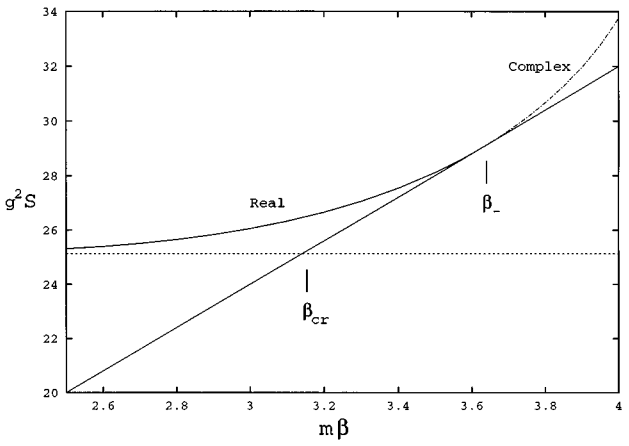


FIG. 4. The action of the periodic instanton and sphaleron as a function of $\beta$ for the O(3) $\sigma$ model. As in Fig. 2, the instanton solution goes from real (solid curve) to complex (dot-dashed curve) at $\beta=\beta_-$, where the sphaleron action $S=E_{\rm sph}\beta$ is tangent to the curve. However, in contrast with Fig. 2 the value of $\beta_{\rm cr}$ at which the sphaleron action equals the zero energy action $2S_0$ (dashed horizontal line) is less than $\beta_-$.

$$C=\frac{2}{\pi}\int_0^\infty dx\left[\frac{1}{x^2+1}+\frac{1}{x^2+4}\right]\ln(x^2+1)=\ln 12=2.4849. \tag{3.19}$$

As a result, the constant defined in Eq. (5.17) of Ref. [16] changes as well, becoming $K=2e^C/\sqrt{3}=8\sqrt{3}=13.8564$.

The sphaleron thermal activation rate (3.15) is less than the instanton-mediated tunneling rate unless $T>T_{\rm cr}$ where the crossover temperature,

$$T_{\rm cr}=\frac{m}{\pi}>T_-=\sqrt{\frac{3}{2}}\frac{m}{\pi}, \tag{3.20}$$

is defined by equating the quantum tunneling and thermal activation exponents, $2S_0=E_{\rm sph}/T_{\rm cr}$. Hence, although the sphaleron provides a second semiclassical escape path for winding number transitions for all temperatures above $T_-$, its contribution is exponentially subdominant until the temperature $T\geqslant T_{\rm cr}>T_-$ where there is a *sharp crossover* from quantum tunneling mediated by the zero scale singular instanton to thermal activation via the static sphaleron, in the semiclassical weak coupling approximation $g^2\ll 1$.

The fact that the crossover between winding number transitions dominated by quantum tunneling and those dominated by thermal activation takes place at a temperature $T_{\rm cr}$ greater than that at which the $n=1$ eigenvalue (3.14) goes through zero is a qualitative difference from the situation in one-dimensional quantum mechanics or the Abelian Higgs model in $1+1$ dimensions. In each of these examples the temperature at which the sphaleron and instanton–anti-instanton exponents are equal is *smaller* than the corresponding $T_-$ of the sphaleron negative mode. In such cases the crossover between zero temperature quantum tunneling and finite temperature thermal activation is smooth and the sphaleron dominates the transition rate for all $T\geqslant T_-$. The situation for the O(3) $\sigma$ model is illustrated in Fig. 4 where the numerical results from Sec. V are incorporated.

As is easy to see from scaling arguments (Derrick's theorem), the mass term $S_m$ now drives the instanton size $\rho\to 0$, so there is no exact instanton of the form (3.7) except the singular one with $\rho=0$. However, for small but finite $\rho$ the instanton configuration (3.7) remains an approximate solution for $r\ll m^{-1}$. Furthermore, for $r\gg\rho$, $|w_0|\ll 1$ and the field equations linearize for any $m$. Hence, if $m\rho\ll 1$ a smooth field configuration which is an approximate solution for all $r$ is

$$w_m(x,\tau)=m\rho e^{-i\theta}K_1(mr), \tag{3.21}$$

where the Bessel function $K_1$ is the solution of the linearized Euler-Lagrange equations obeying the boundary condition at infinity. This approximate solution with action close to the instanton action $4\pi/g^2$ contributes to the winding number vacuum-to-vacuum transition amplitude just as the exact instanton (3.7) solution does in the symmetric $m=0$ model.

In either the softly broken or unbroken $\sigma$ model instanton–anti-instanton configurations are also approximate solutions to the field equations with finite energy. In the low energy regime, perturbation theory is valid and one can construct the approximate solutions by forming an infinite chain of alternating instantons and anti-instantons along the Euclidean time axis separated by a half period $\beta/2$. At this point a new parameter, the period $\beta$ enters the problem and we have a finite interaction between instantons and anti-instantons along the chain, just as in the pendulum example of the previous section. Hence, we can have a competition between the tendency of the scale $\rho$ to shrink to zero for an instanton in isolation and the tendency of $\rho$ to increase due to the attractive interaction between neighboring instantons and anti-instantons, with the two effects balanced at a particular $\rho$ which is a function of $\beta$. In order to obtain some detailed understanding of this qualitative picture and provide a quantitative benchmark for the numerical methods to follow, we work out in the next section the periodic instanton solution for energies $E\ll E_{\rm sph}$ where perturbative methods are applicable.

## IV. LOW ENERGY PERTURBATION THEORY

Our construction of the periodic instanton solution at low energies will take place in two steps. Since we are not in possession of an exact solution to the classical equations for finite $m\rho$ we evaluate the action of the configuration (3.21) to first nonvanishing order in $m\rho$, at first without regard to the finite periodicity $\beta$. Then, we proceed to patch the configurations together to construct a trial configuration periodic in Euclidean time as in the pendulum example. Extremizing the resulting action function with respect to the free scale parameter $\rho$ will determine the particular $\rho(\beta)$ at which the attractive interaction between instantons and anti-instantons just balances the self-interaction which would cause an instanton to shrink to zero size in isolation. Provided that in the end $m\rho(\beta)\ll 1$, the expansion is consistent and we may trust the resulting extremal action constructed in this way as the correct periodic instanton action to first nonvanishing order in the small parameter $m\rho(\beta)$, or equivalently $E/E_{\rm sph}$.

The $\sigma$ model action for any function of the form $w(x,\tau)=e^{-i\theta}f(r)$ may be expressed as

$$S=\frac{4\pi}{g^2}\int_0^\infty rdr\left[\frac{(f'^2+f^2/r^2)}{(1+f^2)^2}+\frac{m^2f^2}{(1+f^2)}\right]. \tag{4.1}$$

For the trial configuration $f=m\rho K_1(mr)$ we make use of the Bessel function identity, $K_1'+K_1/u=-K_0$, to rewrite the first integral in the preceding expression in the form,

$$m^2\rho^2\int_0^\infty udu\,\frac{[K_0^2(u)-2K_1K_1'/u]}{[1+m^2\rho^2K_1^2(u)]^2}. \tag{4.2}$$

Let us divide the integration over $u\equiv mr$ into two parts, $u\leqslant a$ and $u\geqslant a$ where $a$ is chosen so that $m\rho\ll a\ll 1$ in the limit of small $m\rho$. For $u\leqslant a$ we can make use of the series expansions of the Bessel functions for small argument,

$$K_0(u)=-\left[\ln\left(\frac{u}{2}\right)+\gamma_E\right][1+O(u^2)],$$

$$K_1(u)=\frac{1}{u}+\frac{u}{2}\left[\ln\left(\frac{u}{2}\right)+\gamma_E-\frac{1}{2}\right][1+O(u^2)],$$

$$K_2(u)=\frac{2}{u^2}-\frac{1}{2}+O(u^2\ln u), \tag{4.3}$$

taking care to include all terms that give a contribution to the final answer up to order $m^2\rho^2$, while in the interval $u\geqslant a$ we can safely replace the denominator in Eq. (4.2) by unity since the terms neglected are higher order in $m^2\rho^2$ and the integral with lower cutoff $a$ is nonsingular. In this way we find

$$\begin{aligned}I_1&\equiv\int_0^a udu\,\frac{[K_0^2(u)-2K_1K_1'/u]}{[1+m^2\rho^2K_1^2(u)]^2}\\&=-\frac{1}{a^2}+\frac{1}{m^2\rho^2}-\ln\left(\frac{a}{2}\right)-\gamma_E+\frac{1}{2}\\&\quad+O(m^2\rho^2\ln^2 m\rho,a^2\ln^2 a)\end{aligned} \tag{4.4}$$

and

$$\begin{aligned}I_2&\equiv\int_a^\infty udu\,\frac{[K_0^2(u)-2K_1K_1'/u]}{[1+m^2\rho^2K_1^2(u)]^2}\\&=\frac{1}{a^2}+\ln\left(\frac{a}{2}\right)+\gamma_E+O(m^2\rho^2\ln^2 m\rho,a^2\ln^2 a),\end{aligned} \tag{4.5}$$

where $\gamma_E=0.577\ldots$ is Euler's constant. In the latter integral we have made use of the integration formula 5.54(2) of Ref. [18],

$$\int_a^\infty udu K_0^2(u)=-\frac{a^2}{2}[K_0^2(a)-K_1^2(a)]. \tag{4.6}$$

Combining the results (4.4) and (4.5), the $a$ dependence drops out (as it must) and we obtain

$$I_1+I_2=\frac{1}{m^2\rho^2}+\frac{1}{2}+O(m^2\rho^2\ln^2 m\rho). \tag{4.7}$$

Analyzing the second integral in Eq. (4.1) in the same way, we obtain

$$\begin{aligned}I_3&\equiv\int_0^a\frac{udu K_1^2(u)}{[1+m^2\rho^2K_1^2(u)]}\\&=\ln a-\ln m\rho+O(m^2\rho^2\ln^2 m\rho,a^2\ln^2 a)\end{aligned} \tag{4.8}$$

and

$$\begin{aligned}I_4&\equiv\int_a^\infty\frac{udu K_1^2(u)}{[1+m^2\rho^2K_1^2(u)]}\\&=-\ln\left(\frac{a}{2}\right)-\gamma_E-\frac{1}{2}+O(m^2\rho^2\ln^2 m\rho,a^2\ln^2 a),\end{aligned} \tag{4.9}$$

where in this latter integral we have made use of the integration formula,

$$\int_a^\infty udu K_1^2(u)=\frac{a^2}{2}[K_0(a)K_2(a)-K_1^2(a)]. \tag{4.10}$$

Hence, we find

$$I_3+I_4=-\ln\left(\frac{m\rho}{2}\right)-\gamma_E-\frac{1}{2}+O(m^2\rho^2\ln^2 m\rho), \tag{4.11}$$

and all together the action of the trial configuration is

$$\begin{aligned}S[w_m]&=\frac{4\pi m^2\rho^2}{g^2}(I_1+I_2+I_3+I_4)\\&=\frac{4\pi}{g^2}\left\{1-m^2\rho^2\left[\ln\left(\frac{m\rho}{2}\right)+\gamma_E\right]+O(m^4\rho^4\ln^2 m\rho)\right\}.\end{aligned} \tag{4.12}$$

The leading $4\pi/g^2$ term is clearly the one instanton action of the unbroken $(m=0)$ model, so that in considering periodic instantons next we should multiply the result (4.12) by two.

In order to calculate the corrections to the action due to the finite periodicity in the $\sigma$ model we follow the same method as in the pendulum example. We consider the periodic configuration

$$w(\tau,x)=\begin{cases}w_m(\tau,x), & 0\leqslant\tau\leqslant\beta/4,\\ w_m\left(\frac{\beta}{2}-\tau,x\right), & \beta/4\leqslant\tau\leqslant 3\beta/4,\\ w_m(\tau-\beta,x), & 3\beta/4\leqslant\tau\leqslant\beta,\end{cases} \tag{4.13}$$

and evaluate its action in the fundamental interval $[0,\beta]$ to first nontrivial order in $m^2\rho^2$. Starting from

$$S=\frac{2}{g^2}\int_0^\beta d\tau\int_{-\infty}^\infty dx\left\{\frac{|\partial_\tau w|^2+|\partial_x w|^2}{(1+|w|^2)^2}+m^2\frac{|w|^2}{1+|w|^2}\right\}, \tag{4.14}$$

the $\beta$ dependence of the action comes from the tail of the configuration where $|w|\ll 1$, and hence to leading order in $m^2\rho^2$ the $|w|^2$ terms in the denominators may be neglected. By introducing the spatial Fourier transform [19],

$$\widetilde{w}_m(\tau,k)\equiv\int_{-\infty}^{\infty}dx e^{ikx}w_m(\tau,x)$$

$$=-2im\rho\int_0^{\infty}\frac{dx}{r}(\tau\cos kx-x\sin kx)K_1(mr)$$

$$=-i\frac{\pi\rho}{\omega_k}(\omega_k-k)\exp(-|\tau|\omega_k), \tag{4.15}$$

we find that the $\beta$-dependent part of $S$ may be expressed in the form

$$\frac{\partial S}{\partial\beta}=\frac{8}{g^2}\frac{\partial}{\partial\beta}\int_0^{\beta/4}d\tau\int_{-\infty}^{\infty}\frac{dk}{2\pi}\{|\partial_\tau\widetilde{w}_m(\tau,k)|^2+\omega_k^2|\widetilde{w}_m(\tau,k)|^2\}$$

$$=\frac{4\pi\rho^2}{g^2}\int_0^{\infty}dk(\omega_k^2+k^2)\exp\left(-\frac{\beta\omega_k}{2}\right) \tag{4.16}$$

to leading order in $m^2\rho^2$. The infinite periodicity, $\beta$-*in*dependent part of $S$, cannot be evaluated from only the quadratic terms in the action but it is just given by twice the zero energy action we calculated in Eq. (4.12) above. Hence,

$$S[w]=\frac{8\pi}{g^2}\left\{1-m^2\rho^2\left[\ln\left(\frac{m\rho}{2}\right)+\gamma_E\right]-\rho^2\int_0^{\infty}dk\frac{(\omega_k^2+k^2)}{\omega_k}\right.$$

$$\left.\times\exp\left(-\frac{\beta\omega_k}{2}\right)+O(m^4\rho^4\ln^2 m\rho)\right\} \tag{4.17}$$

is the action of the configuration (4.13) to this order.

As in the pendulum example of the last section, the joining of the configurations at $\tau=\beta/4$ and $\tau=3\beta/4$ produces delta function source terms proportional to

$$L[w]\equiv\left(-\frac{\partial^2}{\partial\tau^2}-\frac{\partial^2}{\partial x^2}+m^2\right)w(\tau,x)$$

$$=-2\partial_\tau w_m\left(\frac{\beta}{4},x\right)\delta\left(\tau-\frac{\beta}{4}\right)$$

$$+2\partial_\tau w_m\left(-\frac{\beta}{4},x\right)\delta\left(\tau-\frac{3\beta}{4}\right). \tag{4.18}$$

Making use of the periodic thermal propagator in two dimensions,

$$G_\beta(\tau,\tau';x,x')=\int_{-\infty}^{\infty}\frac{dk}{2\pi}\frac{1}{2\omega_k}\frac{e^{ik(x-x')}}{\sinh(\beta\omega_k/2)}$$

$$\times\cosh\omega_k\left(|\tau-\tau'|-\frac{\beta}{2}\right) \tag{4.19}$$

and taking account of the two real degrees of freedom in the complex field $w$, we obtain the quadratic shift in the action:

$$\frac{2}{g^2}\int d\tau\int d\tau'\int dx\int dx' L'[w^*]G_\beta(\tau,\tau';x,x')L[w]. \tag{4.20}$$

Substituting Eqs. (4.18) and (4.19) into this expression, we find that the quadratic shift becomes

$$\frac{4}{g^2}\int_0^{\infty}\frac{dk}{\pi\omega_k}\left\{\left|\partial_\tau\widetilde{w}_m\left(\frac{\beta}{4},k\right)\right|^2\coth\left(\frac{\beta\omega_k}{2}\right)\right.$$

$$\left.-\frac{1}{\sinh(\beta\omega_k/2)}\partial_\tau\widetilde{w}_m^*\left(\frac{\beta}{4},k\right)\partial_\tau\widetilde{w}_m\left(-\frac{\beta}{4},k\right)\right\}. \tag{4.21}$$

We did not need to keep the analogue of the second term above in the pendulum model since there it is subdominant to the first term as $\beta\to\infty$. However, in the O(3) model $\beta\to 0$ as $E\to 0$ as we shall see presently, and this second term must be retained as well.

Since from Eq. (4.15),

$$\partial_\tau\widetilde{w}_m\left(\pm\frac{\beta}{4},k\right)=i\pi\rho(\omega_k\mp k)\exp\left(-\frac{\beta\omega_k}{4}\right), \tag{4.22}$$

the quadratic correction to the action arising from the shift (4.20) is

$$-\frac{8\pi\rho^2}{g^2}\int_0^{\infty}\frac{dk}{\omega_k}\frac{1}{\sinh(\beta\omega_k/2)}$$

$$\times\left[k^2(1+e^{-\beta\omega_k})-\frac{m^2}{2}(1-e^{-\beta\omega_k})\right]. \tag{4.23}$$

Combining this shift with the unshifted action (4.17) we secure, finally,

$$S(\beta,\rho)=\frac{8\pi}{g^2}\left\{1-m^2\rho^2\left[F(m\beta)+\ln\left(\frac{m\rho}{2}\right)+\gamma_E\right]\right\} \tag{4.24}$$

to the lowest nontrivial order in $m\rho$, where

$$F(m\beta)\equiv\int_0^{\infty}\frac{dk}{\omega_k}\frac{1}{\sinh(\beta\omega_k/2)}\left[\frac{2k^2}{m^2}+1-e^{-\beta\omega_k/2}\right]>0\,. \tag{4.25}$$

This result may also be obtained by the ''$R$-term'' method [7,10].

With the action of the trial configuration in hand for arbitrary small $m\rho$ we can determine the value of $\rho$ which extremizes the action and, therefore, leads to a classical periodic instanton solution close to the trial configuration (4.13). Since

$$\frac{\partial S(\beta,\rho)}{\partial\rho}=-\frac{8\pi m^2}{g^2}\rho\left[2F+2\ln\left(\frac{m\rho}{2}\right)+2\gamma_E+1\right] \tag{4.26}$$

vanishes for $\rho=0$ or for

$$\rho=\rho(\beta)=\frac{2}{m}\exp[-F(m\beta)-\gamma_E-\tfrac{1}{2}], \tag{4.27}$$

the zero energy singular instanton at $\rho=0$ with finite action $S=8\pi/g^2$ is always a solution of the equations for any period $\beta$, but there is also a nontrivial periodic instanton solution with action,

$$S(\beta)=S(\beta,\rho(\beta)) = \frac{8\pi}{g^2}[1+2\exp\{-2F(m\beta)-2\gamma_E-1\}]>\frac{8\pi}{g^2}, \tag{4.28}$$

and energy,

$$E(\beta)=\frac{dS}{d\beta} =-\frac{32\pi m}{g^2}\exp[-2F(m\beta)-2\gamma_E-1]F'(m\beta) =\frac{16\pi e^{-2\gamma_E-1}}{g^2}e^{-2F}\int_0^\infty \frac{dk}{\sinh^2(\omega_k\beta/2)} \times\left\{\left(\frac{2k^2}{m^2}+1\right)\cosh\left(\frac{\omega_k\beta}{2}\right)-1\right\}. \tag{4.29}$$

This second nonsingular solution with nonzero $\rho(\beta)$ is the periodic instanton solution we seek in the limit of small but finite $E$.

The qualitative picture sketched in the previous section has been verified by this explicit calculation, namely, at the nontrivial value of $\rho(\beta)$ in Eq. (4.27), the tendency of an individual instanton or anti-instanton to contract to $\rho=0$, represented by the logarithm in Eq. (4.26) is just balanced by the attractive interaction between members of the infinite chain which tends to increase $\rho$, represented by the $F(m\beta)$ term in Eq. (4.26). This competition between the two effects can occur in the $\sigma$ model only because of the softly broken conformal invariance of the mass term $S_m$ which leads to the existence of the conformal scale parameter $\rho$.

Notice also that in contrast with the pendulum example of the last section it is *not* $\beta\to\infty$ which characterizes the low energy limit $E\to 0$, but rather $F(m\beta)\to\infty$ in the $\sigma$ model. Since $F(m\beta)$ vanishes exponentially as $\beta\to\infty$ but in the opposite limit,

$$F(m\beta)\to\frac{\pi^2}{m^2\beta^2}\to\infty \quad \text{as} \quad m\beta\to 0\,, \tag{4.30}$$

the low energy limit is characterized by $\beta\to 0$. This (possibly counterintuitive) result is, nevertheless, consistent with perturbation theory and the dilute gas picture of instantons and anti-instantons at low energies because the size of the individual (anti-)instantons goes to zero much more rapidly with $\beta\to 0$, and it is the ratio

$$\frac{\rho(\beta)}{\beta}\to\frac{2e^{-\gamma_E-1/2}}{m\beta}\exp\left(-\frac{\pi^2}{m^2\beta^2}\right)\to 0 \tag{4.31}$$

which controls the validity of the dilute gas approximation. Clearly then, as $\beta\to 0$, $\rho(\beta)\to 0$ exponentially, and it is legitimate to neglect the higher powers of $m\rho$ in Eq. (4.29) in the low energy limit, $E\ll E_{\rm sph}$, which justifies our expansion in powers of $m\rho$ *a posteriori*. In the extreme low energy limit we have the asymptotic forms

$$S(\beta)\to\frac{8\pi}{g^2}\left[1+\frac{2}{e^{2\gamma_E+1}}\exp\left(-\frac{2\pi^2}{m^2\beta^2}\right)\right],$$

and

$$E(\beta)\to\frac{64\pi^3}{g^2e^{2\gamma_E+1}m^2\beta^3}\exp\left(-\frac{2\pi^2}{m^2\beta^2}\right). \tag{4.32}$$

From either this last expression or the more accurate Eq. (4.29) above we find that the behavior of $E$ increasing with increasing $\beta$,

$$\frac{dE}{d\beta}>0 \tag{4.33}$$

is actually the case for the periodic instantons in the low energy limit of the nonlinear $\sigma$ model. We shall see in the next section that this behavior persists for all energies up to the sphaleron energy. Hence, it is already clear that the behavior of the periodic instantons in the O(3) model is very different from that of systems with only one quantum-mechanical degree of freedom such as the simple pendulum, or the Abelian Higgs model. In those models $\beta(E)\to\infty$ as $E\to 0$, and the periodic instanton contributes to the transition rate as the temperature $\beta^{-1}$ goes smoothly to zero. From the discussion at the end of Sec. II it follows that these periodic instantons in the $\sigma$ model with period going to *zero* as $E\to 0$ cannot contribute to the low temperature transition rate, although they can contribute to, and in fact dominate, transitions between *non*thermal low *energy* states.

Clearly, this behavior is a direct consequence of the conformal invariance of the unbroken model which leads to the additional scale parameter $\rho$ in the instanton configuration, and as it turns out, an additional negative mode direction in the fluctuations around this configuration. This additional negative mode is easily checked from the second derivative of the classical action (4.24),

$$\left.\frac{\partial^2 S}{\partial\rho^2}\right|_{\rho=\rho(\beta)} =-\frac{8\pi m^2}{g^2}\left[3+2\gamma_E+2\ln\left(\frac{m\rho}{2}\right)+2F(m\beta)\right]\Bigg|_{\rho=\rho(\beta)} =-\frac{16\pi}{g^2}m^2<0, \tag{4.34}$$

on the solution with nonzero $\rho(\beta)$. Thus, any small change of $\rho$ from its critical value, $\rho(\beta)$ *decreases* the action of the configuration and implies the existence of a negative eigenvalue in the second order fluctuation operator around the nonsingular periodic instanton solution that is quite independent of the usual negative mode with fixed $\rho$ as found by the standard argument of Sec. II. The origin of this second negative mode about the nontrivial periodic instanton solution we have found for low $E$ should be clear from what has already been said regarding the balance between the attractive interaction between nearest-neighbor instantons and anti-instantons on the one hand, and the self-interaction attracting each individual (anti-)instanton towards zero size on the other. If the precise balance between the two is upset by

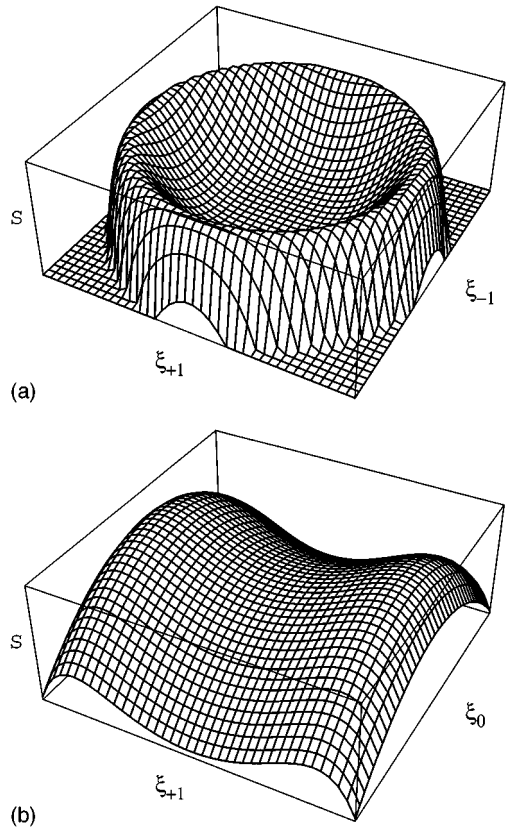


FIG. 5. The action $S$ plotted as a function of the same variables $\xi_{\pm 1}$ (a), and $\xi_0$ (b), for fixed $\beta<\beta_-$, as in Fig. 3, but for the O(3) $\sigma$ model. The periodic instanton is again represented by the ring of extrema of $S$ in (a) or the two outer extrema in (b), which merge with the sphaleron in the center as $\beta$ approaches $\beta_-$. Since the periodic instanton solution now has two negative modes and higher action than that of the sphaleron, it is subdominant. The finite temperature winding number transition goes over the lowest saddle, either the sphaleron or the $\rho=0$ instanton (not shown) depending on the temperature.

varying $\rho$ slightly away from its critical value, $\rho(\beta)$, then one or the other of the two interactions dominates and $\rho$ is driven further away from its critical value, i.e., there is a negative mode in the direction of varying $\rho$, which is just what Eq. (4.34) makes explicit.

It is this second negative mode direction due to conformal rescalings that makes the nontrivial periodic instanton configuration subdominant at finite temperature, at least in the low energy limit where perturbation theory and the form (4.29) apply. Correspondingly, the periodic instanton action (4.28) is *greater* than the singular solution with $\rho=0$. Near the sphaleron energy the action as a function of the three relevant variables $\xi_{\pm 1}$ and $\xi_0$ for the $\sigma$ model is illustrated in Fig. 5.

From the first form of Eq. (4.34) we observe that the zero size instanton–anti-instanton configuration has no second negative mode in the $\rho$ direction. It has only the expected single negative mode corresponding to the attractive interaction between the pair. Hence, this singular configuration with fixed finite action per period $2S_0$ (shown as the constant straight line in Fig. 4) can and does contribute to the winding number transition rate at low temperature $T<T_{\rm cr}$. Notice from Fig. 4 that although the actions $2S_0$ and $E_{\rm sph}\beta$ are equal at $\beta=1/T_{\rm cr}$ the actual field configurations of the zero size instanton–anti-instanton pair and the sphaleron are quite different and there is no merging of these solutions at $\beta=\beta_{\rm cr}$.

The picture we have sketched in this section is based on the existence of a perturbative instanton–anti-instanton expansion at low energies and knowledge of the sphaleron and its negative mode at finite energy and $\beta$ near $\beta_{\rm cr}$. Continuity of the space of solutions to the classical Euclidean equations suggests that the periodic instanton solutions merge with the sphaleron as $\beta$ approaches $\beta_{\rm cr}$ from below with $dE/d\beta>0$. However, one does not know how the action and energy of these solutions will vary as $\beta$ is varied from $\beta_{\rm cr}$ *a priori*. In the absence of analytic methods for finding the periodic instanton solutions to the Euclidean equations in the intermediate region between $E\to 0$ where perturbation theory holds and $E\to E_{\rm sph}$ where the solutions approach the static sphaleron, one must rely on a numerical approach. It is to the details and results of this numerical study which justifies Figs. 4 and 5 that we turn next.

## V. NUMERICAL TECHNIQUE AND RESULTS

In this section we present the results of a numerical study of periodic instanton solutions in the two-dimensional, nonlinear O(3) $\sigma$ model modified by the mass term $S_m$. A preliminary version of these results has been reported earlier in Ref. [20]. At energies comparable, but not very close to the sphaleron energy, the periodic instanton solution has to be found numerically, i.e., one must solve the Euclidean field equations,

$$-(\partial_\tau^2+\partial_x^2)n^a+m^2\delta_3^a-\alpha n^a=0, \tag{5.1}$$

together with the constraint,

$$n^a n^a=1\,. \tag{5.2}$$

Here, $\alpha$ is a Lagrange multiplier enforcing the constraint, which is easily found by multiplying Eq. (5.1) by $n^a$ and using Eq. (5.2): namely,

$$\alpha=-n^a(\partial_\tau^2+\partial_x^2)n^a+m^2n_3=\partial_\mu n^a\partial_\mu n^a+m^2n_3\,. \tag{5.3}$$

The periodic instanton solution we seek has vanishing time derivative at initial time $\tau=0$, and it evolves to another turning point at half-period $\beta/2$ where it reflects and then returns to its initial configuration at $\tau=\beta$ by simply reversing the sign of all $\tau$ derivatives. Thus, we enforce the half-period boundary conditions,

$$\frac{\partial n^a(\tau=0,x)}{\partial\tau}=\frac{\partial n^a(\tau=\beta/2,x)}{\partial\tau}=0, \tag{5.4}$$

which remove the time translation invariance of the solution. The other boundary condition we require is that at spatial infinity the solution approaches the vacuum. Since we shall work in a finite box of length $L$ we require

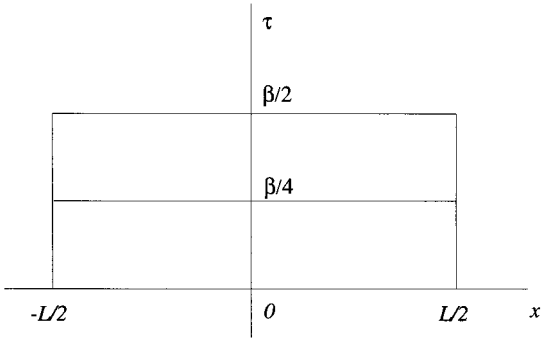


FIG. 6. The finite rectangular region $(\tau,x)$ of coordinate space that maps onto the shaded region of the sphere in Fig. 7.

$$n^a(\tau,x=-L/2)=n^a(\tau,x=L/2)=n^a_{(\mathrm{vac})}=(0,0,-1) \tag{5.5}$$

for $mL$ large but finite.

Geometrically, the periodic instanton solution obeying these boundary conditions maps the rectangular region of $(\tau,x)$ coordinate space pictured in Fig. 6 into the shaded region of the sphere in Fig. 7. From these figures it should be clear that the solution may be chosen to have well-defined symmetry properties under reflection through the lines bisecting the rectangular region of Fig. 6, so that at $x=0$, $n_1$ vanishes while $n_2$ and $n_3$ reach extrema, and at $\tau=\beta/4$, $n_2$ vanishes while $n_1$ and $n_3$ reach extrema. Imposing these symmetries fixes completely the spatial translational invariance and rotation invariance around the $n_3$ axis of the solution, as well as reduces the region we must consider to only one-quarter of the full rectangle in Fig. 6. Hence, we solve the differential Eq. (5.1) subject to the boundary conditions

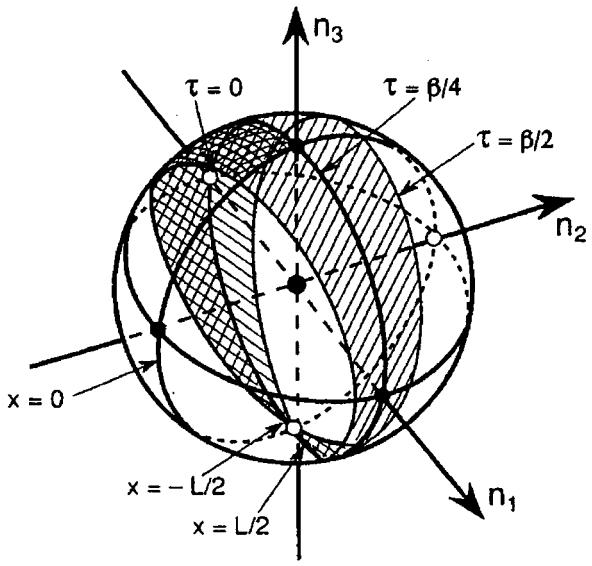


FIG. 7. Geometric representation of the periodic instanton range on $S^2$.

$$\begin{aligned}
&x=-L/2: \quad n_1=0; \quad n_2=0; \quad n_3=-1;\\
&\tau=0: \quad dn_1/d\tau=dn_2/d\tau=dn_3/d\tau=0;\\
&x=0: \quad n_1=0; \quad dn_2/dx=dn_3/dx=0;\\
&\tau=\beta/4: \quad n_2=0; \quad dn_1/d\tau=dn_3/d\tau=0.
\end{aligned} \tag{5.6}$$

The lattice version of Eq. (5.1) can be obtained by a variational principle starting from the discretized action. Let $(\tau_i,x_j)$, where $i=0,\ldots,I$ and $j=0,\ldots,J$, be the coordinates of lattice sites. The lattice version of the actions (3.1) and (3.10) read

$$S=\sum_{i,j}\left\{\frac{1}{2}(n^a_{i+1,j}-n^a_{ij})^2\frac{d\tilde{x}_j}{d\tau_i}+\frac{1}{2}(n^a_{i,j+1}-n^a_{ij})^2\frac{d\tilde{\tau}_i}{dx_j}+m^2(1+n^3_{ij})d\tilde{\tau}_i d\tilde{x}_j\right\} \tag{5.7}$$

where we have used the notation $d\tau_i=\tau_{i+1}-\tau_i$, $d\tilde{\tau}_i=(1/2)(d\tau_{i-1}+d\tau_i)$ and similarly, for $dx_j$, $d\tilde{x}_j$.

The equations which follow from the action (5.7) can be written in the form

$$[B^a-n^a(B^b n_b)]_{ij}=0, \tag{5.8}$$

where

$$B^a_{ij}\equiv-\frac{n^a_{i+1,j}}{d\tilde{\tau}_i d\tau_i}-\frac{n^a_{i-1,j}}{d\tilde{\tau}_i d\tau_{i-1}}-\frac{n^a_{i,j+1}}{d\tilde{x}_j dx_j}-\frac{n^a_{i,j-1}}{d\tilde{x}_j dx_{j-1}}+m^2\delta_{a3}. \tag{5.9}$$

Equation (5.8) actually contains only two independent equations since its projection onto the vector $n^a_{ij}$ is identically zero. Together with the constraint equation (5.2), these comprise a complete set of three independent equations associated with each lattice site. From Eqs. (5.8) and (5.9) it is clear that $B^a$ must be antiparallel to $n^a$ at each point $(i,j)$. Since $n^a$ is normalized to unity, the Eqs. (5.8) and (5.9) can be rewritten in the equivalent, symmetric form,

$$n^a\sqrt{B^cB^c}+B^a=0, \tag{5.10}$$

for every $(i,j)$, and where the negative sign of the square root has to be taken because $n_aB^a<0$. This form is most convenient for numerical calculations.

To obtain a numerical solution of Eq. (5.10) we use Newton's method [21]. That is, we (1) choose an initial field configuration as a first guess, (2) linearize the equation (5.10) in the background of the initial field, (3) solve the linearized equation to obtain an improved configuration, and (4) iterate until the procedure converges.

The third step above also involves a renormalization: the improved configuration after every Newton step is locally scaled to ensure that at every lattice point the constraint (5.2) is satisfied. This procedure speeds up the convergence to the final solution. The numerical solutions were found for $m=1=g$.

The choice of initial configuration is guided by the known behavior of the periodic instanton solution near $E=0$ and $E=E_{\mathrm{sph}}$. Consideration of the zero mode in the vicinity of

the sphaleron when $\beta$ approaches $\beta_-$ indicates that we should look for nontrivial periodic solutions of the field equations in the neighborhood of the sphaleron by perturbing the known static solution along the zero mode direction, viz.,

$$n^a_{(\mathrm{sph})}(x) \to n^a_{(\mathrm{sph})}(x) + \delta \cos(|\omega_-|\tau) u^a_-(x), \qquad (5.11)$$

where $\delta$ is a small parameter which goes to zero at $\beta=\beta_-$. Since the classical action function on this solution is identical to Hamilton's principal function, the energy of the solution is given by

$$\frac{dS(\beta)}{d\beta} = E, \qquad (5.12)$$

which must agree with the sphaleron energy $E_{\mathrm{sph}}$ at $\beta=\beta_-$. For $E$ just below $E_{\mathrm{sph}}$ an initial configuration of the form (5.11) with $\delta \sim 0.5$ works well. The convergence of the Newton scheme is quadratic, and depending on the initial starting point, the desired accuracy (an error tolerance of $10^{-10}$ or better) is typically reached in several iterations. Error tolerance limits were set to limit both the maximum violation of the equations of motion at a given lattice site as well as the global error obtained by summing the absolute value of, and then averaging, the errors on all lattice sites. Once the solution has been found at a given $\beta$, we step down (or up) in $\beta$ and use the previous solution as the initial trial configuration for Newton's method at the next value of $\beta$. If the step size in $\beta$ is not too large this procedure enables us to efficiently generate periodic instanton solutions over a finite range of $\beta$.

The solution of the linearized equations in step (3) of the algorithm can be performed by a direct inversion of the matrix of small fluctuations about the trial configuration. (This was the method used in our earlier work on this problem [20] and is described briefly below.) Negative eigenvalues of this matrix are treated on the same footing as positive eigenvalues, and pose no special problem for Newton's method, which is important for the present application. Because of the boundary conditions which fix the translational and rotational symmetries there are no zero eigenvalues of the matrix near the desired solution, which otherwise would be disastrous for this method.

For an $I \times J$ spacetime grid the matrix to be inverted has $I^2J^2$ elements. In general, it takes of order $I^3J^3$ operations to invert such a matrix. However, the sparseness of the matrix makes it more efficient to follow a procedure of forward elimination and back substitution along either the $x$ or $\tau$ directions instead. That is, starting with one edge of the region in Fig. 6, such as $\tau=0$, we can solve for each $\tau$ slice of the grid in terms of the successive two $\tau$ slices until the edge $\tau=\beta/4$ is reached, where the boundary condition determines the unknown quantities. Then we reverse direction and solve for the unknowns on the previous $\tau$ slices successively. This allows for the matrix to be inverted in order $IJ^3$ operations (or $I^3J$ operations if the $x$ direction is chosen), and speeds up the algorithm considerably. In practice, a grid size of order $100 \times 100$ can be handled on a typical work station, which provides reasonable accuracy for configurations not too far from the sphaleron. However, this method rapidly becomes inefficient when large grids are required.

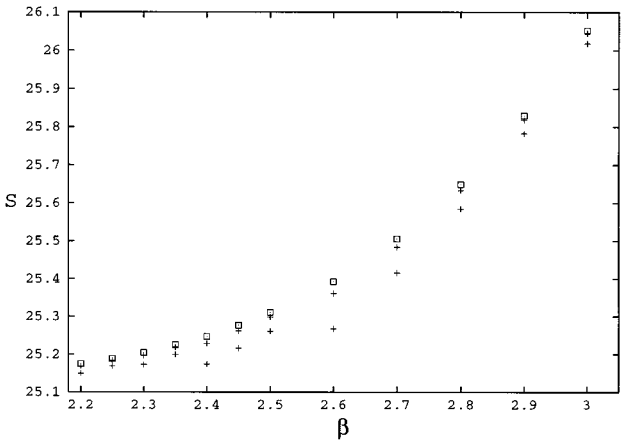


FIG. 8. Action of the periodic instanton as a function of $\beta$ illustrating the improvement due to extrapolation. The two crosses at each $\beta$ are the numerical results from the largest and next-to-largest lattice at that $\beta$ (top and bottom, respectively). The square is the extrapolated point. Accuracy of the extrapolation was checked by extrapolating up from a still coarser, i.e., next-to-next-to-largest lattice and comparing with the actual result at the largest lattice: there was very good agreement in all cases.

The strategy adopted in this paper is to solve the linearized equations using direct matrix methods such as conjugate gradient. The present code allows for the use of several such solvers (all capable of dealing with nonsymmetric, complex matrices). The results reported here were obtained using either the quasiminimized version of Sonneveld's conjugate gradient squared (CGS) algorithm [22] or Van der Vorst's biconjugate gradient with stabilization (BICG-STAB) [23]. The advantage of these methods over matrix inversion is a much less stringent memory requirement [down by a factor of $I$ (or $J$) compared to matrix inversion] and while of the same order algorithmically, typically the prefactor is much smaller. Moreover, the efficient use of a parallel supercomputer becomes possible.

Global grid refinement was used to speed up the method even further, as well as to effectively increase the order of the discretization error. The technique used was to begin with a certain grid size, find the periodic instanton, and then to double the grid size (keeping the physical volume constant) and use an interpolated version of the solution on the smaller grid as the initial guess solution for the bigger lattice. This procedure works as a sort of preconditioner for the matrix solver and since one has the results from the coarser lattice, Richardson extrapolation [24] can be used to reduce the discretization error, effectively improving the second order finite differencing error to third order (Fig. 8). A good check of the error control achieved by the code is energy conservation. Energy error is maximum near $\tau \sim \beta/4$ where the solution is far from the vacuum and varying rapidly in both time and space. An example of the improvement in energy error as a function of grid size (before Richardson extrapolation) is shown in Fig. 9.

In practice, the number of (matrix solver) iterations hardly ever went beyond tens of thousands even for grids as big as of order $1000 \times 1000$ and acceptable accuracies (error tolerances of order $10^{-10}$) were reached in less than four doubling steps starting with configurations of order $100 \times 100$.

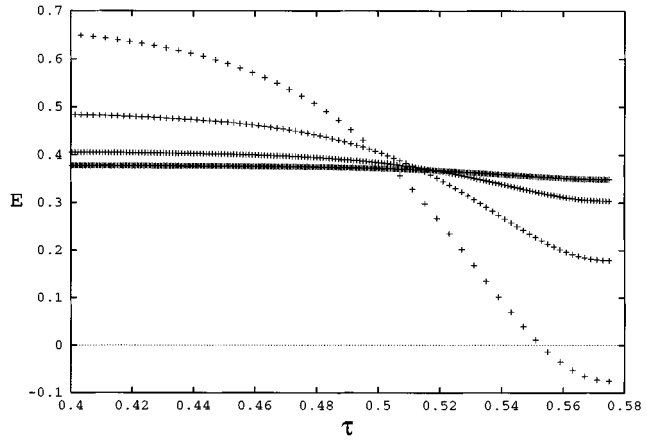


FIG. 9. Energy of the periodic instanton as a function of the time slice at $\beta=2.3$. A small range of $\tau$ is shown to illustrate the improvement in energy conservation as the grid is refined (over four doublings of the grid in this case). Extrapolation improves the result one step further (not shown).

When doing runs for different values of $\beta$, the solution for the previous $\beta$ on the biggest grid was sampled to produce a guess solution for the new $\beta$ on the smallest grid. This allowed efficient scanning of the desired range of $\beta$ values. As will be seen below the numerical results are extremely accurate all the way down to small values of $\beta$ where the perturbative results of the previous section begin to apply.

Without any further optimizations, the new method is already efficient and accurate, yielding a real periodic instanton solution for energies in the range of 0.3 to 8 in units of $m/g^2$. Smaller energies require finer lattices to obtain the same accuracy, since the instanton size becomes smaller rapidly with decreasing $\beta$. Adaptive gridding using either nonuniform grids or selective refinement is possible within the method but was not used as a meaningful comparison with perturbation theory was already possible with the largest grid sizes that were used. (A selective refinement algorithm has been implemented for application to future, more demanding problems.)

The results of the calculations are summarized below. They were obtained on grids as large as $\sim 1200\times 2400$ in spatial boxes with sizes varying from $L=8$ to $L=16$ in units of $m^{-1}$ (for configurations nearer to the sphaleron smaller grids provided sufficient accuracy). For $\beta>\beta_-$, as discussed in the previous section, a real solution does not exist and the solution becomes complex. This complex solution was also found without difficulty by our numerical method. Numerically, the crossover from the real to complex solution occurred between $\beta=3.62$ (real) and $\beta=3.63$ (complex) consistent with $\beta_-=3.628$ (Fig. 4). The action of the complex solution rises steeply at $\beta\approx 4$ and it becomes difficult to track this numerical solution for larger $\beta$ (possible in principle, but not worth the computer time). The numerical results for action and energy vs $\beta$, and $W$ as a function of $E$ are given in Fig. 10. On the scale of the plots, the numerical error estimates are insignificant and are not shown. Comparison with the perturbative results of the previous section shows very good agreement at low values of $\beta$ as expected.

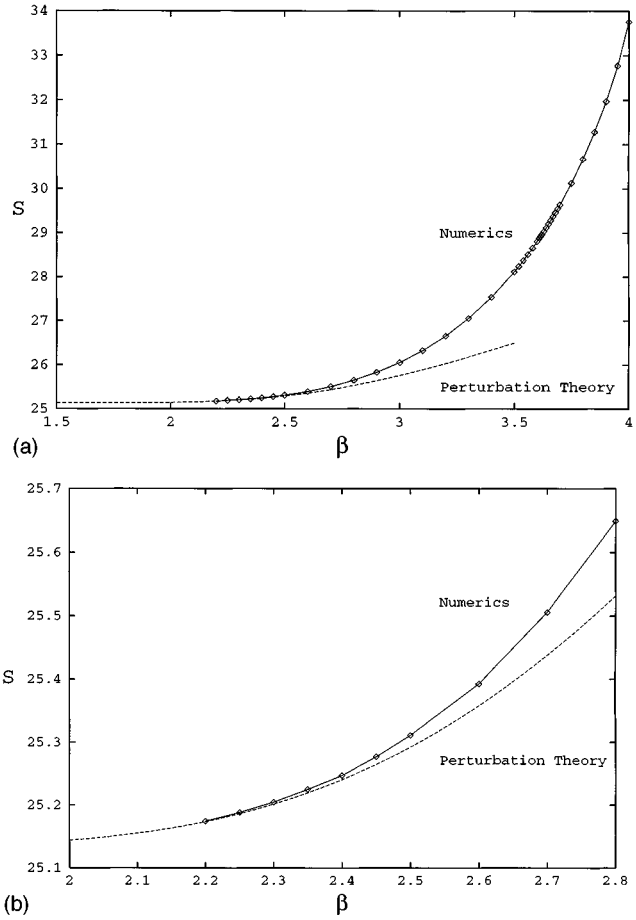


FIG. 10. (a) The action of the periodic instanton as a function of $\beta$. Agreement between the numerics and the perturbation theory [Eq. (4.28), dashed curve] of Sec. IV is excellent in the expected range. (b) The same as (a) but with a more restricted range for $\beta$ in order to better display the comparison with the low energy perturbative expansion (dashed curve) of Eq. (4.28).

This is also illustrated in Fig. 10 by plotting $S$, $E$, and $W$ over a restricted range within which perturbation theory is supposed to become accurate.

From Figs. 10 and 11, it is apparent that the periodic instanton solutions interpolate smoothly between the perturbative region and the sphaleron (see also Fig. 12). In particular, the energy monotonically increases with $\beta$ for the entire range of $\beta$, $[0,\beta_-]$ in accordance with Eq. (1.1).

The numerically evaluated periodic instanton configurations are displayed in Fig. 13 at $\beta=2.8$. These configurations go over to the vacuum solution at the boundary $x=-L/2$ and are strongly nonvacuum near $\tau=\beta/4$, $x=0$. As $\beta$ is lowered, the periodic instanton size goes rapidly to zero (exponentially in the perturbative regime). At lower values of $\beta$, the configurations remain qualitatively similar, but become ever more localized as functions of time and space.

The numerically computed periodic instantons can be compared to the perturbative solution (3.21) with the instanton size $\rho$ given by Eq. (4.27). Since direct comparison is unwieldy and difficult to visualize, we chose to compare the numerical and perturbative values for $|w|$ as a function of $\tau$ at $x=0$. This comparison at $\beta=2.2$ is shown in Fig. 14. As is to be expected, the overall agreement at this low value of

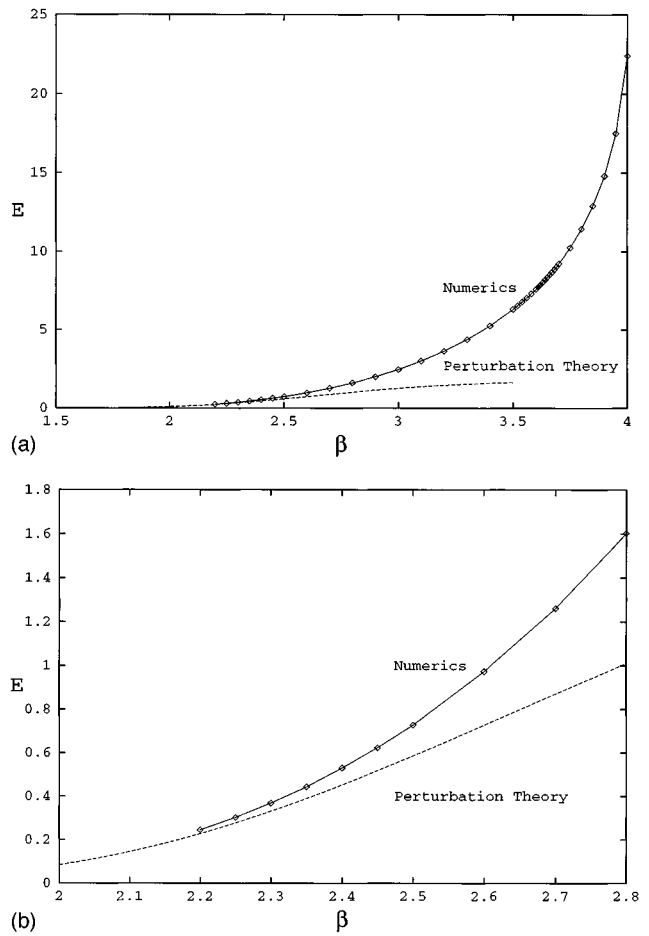


FIG. 11. (a) The energy of the periodic instanton as a function of $\beta$. The dashed curve is the perturbative result, Eq. (4.29). (b) The same as (a) but over a more restricted range of $\beta$.

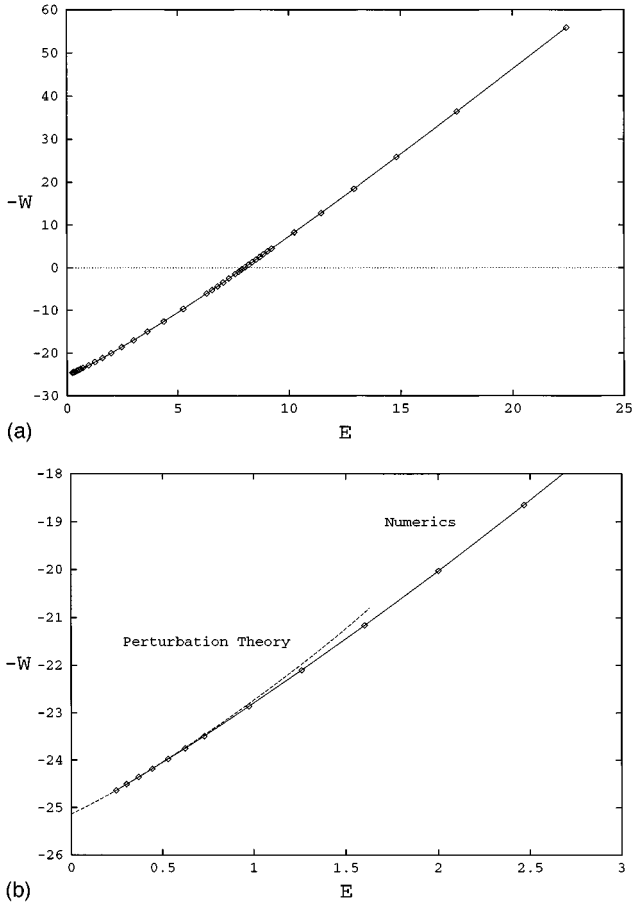


FIG. 12. (a) $-W$ as a function of the energy $E$. The change of sign in $W$ occurs at $E=E_{\rm sph}=8$. (b) The same as (a) but over a more restricted range of $\beta$ in order to display the comparison with the perturbative result (dashed line).

$\beta$ is good. Evidently, perturbation theory underestimates the interactions in the dilute gas chain: the numerical solution has a longer tail and is less sharp than the perturbative configuration near $\tau=\beta/4$.

## VI. SUMMARY AND DISCUSSION

The main conclusion of our study of periodic instanton solutions in the quantum pendulum and the O(3) $\sigma$ model is that two qualitatively and quantitatively different behaviors are possible for these solutions, with correspondingly different physical consequences for finite energy and temperature transitions.

In the first case (I) of which the pendulum is the prototype, the period $\beta$ decreases with increasing energy, $E_{\rm sph}/T_-<2S_0$, the periodic instanton solutions contribute to the finite temperature winding number transition rate, and the crossover from quantum tunneling to thermal activation is smooth:

$$\frac{dE}{d\beta}<0\,;\quad \frac{E_{\rm sph}}{T_-}<2S_0.\ \text{case (I)} \tag{6.1}$$

In addition to the periodic pendulum which we have discussed here in some detail, the symmetric double-well potential,

$$V(q)=\frac{\omega^2}{8}(q^2-1)^2 \tag{6.2}$$

belongs in this class, as may be easily checked from $E_{\rm sph}=V(0)=\omega^2/8$, $T_-=|V''(0)|^{1/2}/2\pi=\omega/2\sqrt{2}\pi$, and the kink action $S_0=2\omega/3$. Hence,

$$\frac{E_{\rm sph}}{T_-}=\frac{\pi\sqrt{2}}{4}\omega<2S_0=\frac{4}{3}\omega, \tag{6.3}$$

and indeed the periodic instanton solutions with the expected behavior are easily found analytically in this example as well.

In two dimensions the most well-studied model possessing both instanton and sphaleron solutions is the Abelian Higgs model, viz.,

$$S=\int d^2x\left\{\frac{1}{4}F_{\mu\nu}^2+|D_\mu\Phi|^2+\lambda\left(|\Phi|^2-\frac{1}{2}v^2\right)^2\right\}. \tag{6.4}$$

It is well known that the instanton solution of this model is an Abrikosov-Nielsen-Olesen vortex of the form [25],

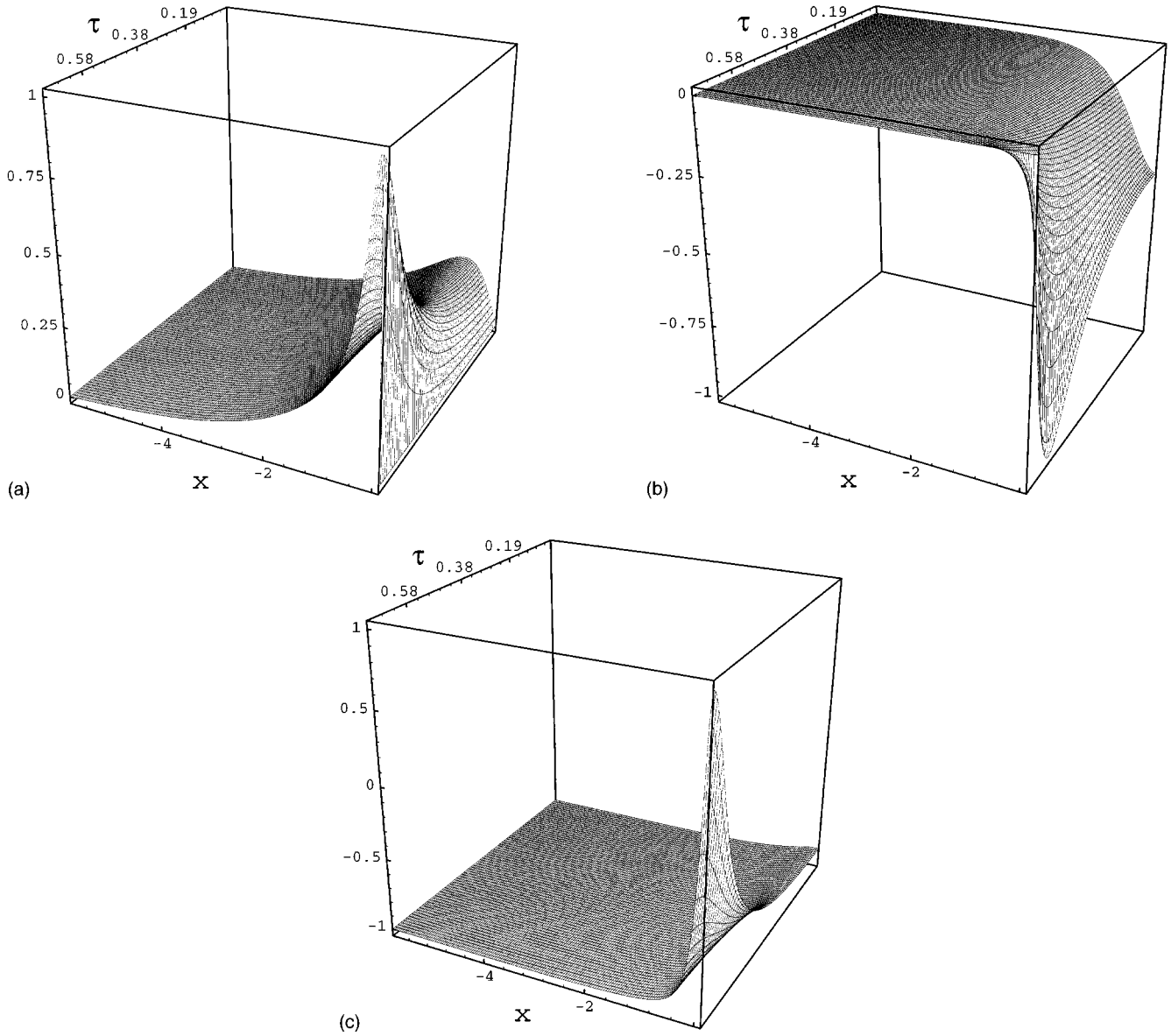


FIG. 13. A typical numerically obtained periodic instanton solution (here at $\beta=2.8$, $L=12$). Shown in the three figures are the Cartesian components of the unit vector $n^1$, $n^2$, and $n^3$ as functions of $\tau$ and $x$ on a $73\times153$ grid ($\tau\times x$). As one can see, at the turning point $\tau=0$ the field configuration is nonvacuum, and the components of the vector $n^a$ cover the shaded patch of the sphere in Fig. 7.

$$A_\mu=\frac{1}{g}\epsilon_{\mu\nu}\frac{x^\nu}{r^2}A(r),$$

$$\Phi=ve^{i\phi}H(r). \tag{6.5}$$

In the special case that $M_H^2=2\lambda v^2$ is taken equal to $M_W^2=g^2v^2$, the vortex may be found analytically, and has the action, $S_0=\pi v^2$. For other values of the ratio $M_H/M_W$ the vortex solution has to be found numerically [26]. The sphaleron and its negative frequency mode are both known analytically for arbitrary values of this ratio [27], viz.,

$$E_{\rm sph}=\frac{2}{3}\sqrt{2\lambda}v^3$$

and

$$\epsilon_-^2=-\frac{\lambda v^2}{4}\left(\sqrt{1+\frac{8g^2}{\lambda}}+1\right). \tag{6.6}$$

Hence, at least in the case $g^2=2\lambda$, we find

$$\frac{E_{\rm sph}}{T_-}=\frac{8\pi\sqrt{2}}{3(\sqrt{17}+1)}v^2<2S_0=2\pi v^2 \tag{6.7}$$

and the two-dimensional Abelian Higgs model also falls into case (I). The periodic instanton solutions have been found numerically in this model for $M_W=M_H$ [28], and they do satisfy Eq. (6.1). In accordance with the intuition gained by our study of the $\sigma$ model, this behavior is the result of the absence of any conformal invariance or scale parameter akin to $\rho$ in the instanton solutions of the Abelian Higgs model, and we would expect this model to behave in the same way

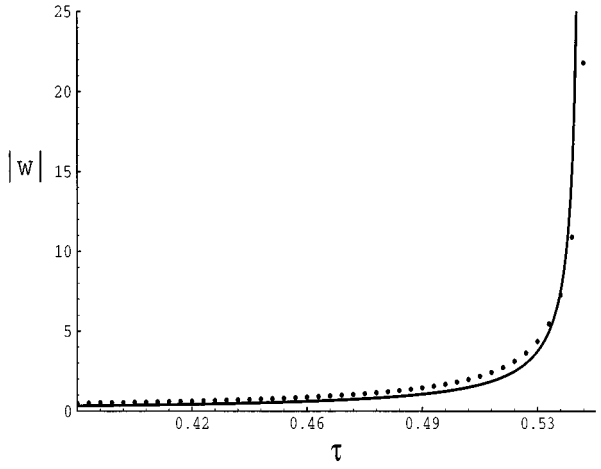


FIG. 14. Comparison of the perturbative (solid line) and numerical results (dots) for $|w|$ as a function of $\tau$ at $x=0$, $\beta=2.2$. Only a small piece of the lattice near $\beta/4=0.55$ is shown for clarity.

for all finite values of the ratio $M_H/M_W$. The numerical results for the vortex action in the literature are consistent with Eq. (6.7) for all values of this ratio.

The O(3) $\sigma$ model is the only example studied so far in any detail which behaves differently: i.e.,

$$\frac{dE}{d\beta}>0\,; \quad E_{\rm sph}/T_{-}>2S_0. \ \text{case (II)} \tag{6.8}$$

In this second case (II), the periodic instanton solutions contribute to the finite *energy* (but *not* to the finite temperature) winding number transition rate, and the crossover from quantum tunneling to thermal activation is sharp, taking place at $T_{\rm cr}>T_{-}$. As we have seen, the key physical differences between cases (I) and (II) appear to be conformal invariance and the scale parameter $\rho$ of the instanton configurations.

These same features are shared by the O(3) $\sigma$ model and four-dimensional gauge theories with spontaneous (and conformal) symmetry breaking arising from the Higgs sector. Indeed, it is interesting to compare the numerical results for the sphaleron energy and negative frequency eigenvalue [29],

| $\frac{M_H}{M_W}$ | $\frac{E_{\rm sph}}{M_W/\alpha_W}$ | $\frac{-\omega^2}{M_W^2}$ | $\frac{E_{\rm sph}\alpha_W}{T_{-}}$ |
|---|---|---|---|
| 0.0 | 3.0405 | 1.318 | 16.64 |
| 0.1 | 3.1384 | 1.486 | 16.18 |
| 1.0 | 3.6417 | 2.460 | 14.59 |
| 2.0 | 3.9532 | 3.257 | 13.76 |
| 3.0 | 4.1633 | 3.967 | 13.13 |
| 4.0 | 4.3179 | 4.667 | 12.59 |
| 5.0 | 4.4375 | 5.405 | 11.99 |
| 7.0 | 4.6115 | 7.176 | 10.82 |
| 10.0 | 4.7805 | 11.21 | 8.97 |

(6.9)

to twice the zero energy instanton action $2S_0$ of the pure SU(2)-Higgs doublet model in four dimensions (which is the standard electroweak model with $\theta_W=0$ and no fermions). Since $2S_0\alpha_W=4\pi=12.566\ldots$, we observe from the last column of the table above that $E_{\rm sph}/T_{-}>2S_0$ for all $M_H/M_W<4.0$ but that the inequality is reversed for all $M_W$ greater than a value slightly larger than $4M_W$. Hence, we conclude that the four-dimensional SU(2)-Higgs doublet model falls under case (II) for $M_H<4M_W$.

Based on our study of instanton solutions in this paper we are led to suspect that the four-dimensional gauge theory is similar to the O(3) model, for not too large Higgs self-coupling. Indeed, since SU(2) pure gauge theory is conformally invariant, there is an instanton scale parameter $\rho$, which is driven to zero by the addition of the Higgs sector with its conformal-breaking expectation value $v$. Hence the instanton or anti-instanton solution no longer exists in isolation for a nonzero Higgs boson mass $M_H=\sqrt{2\lambda}v$. However, the interaction between instantons and anti-instantons is again attractive, so that at finite periodicity $\beta$ there is an opposing interaction, and it is possible to balance the two interactions at a definite value of $\rho(\beta)$, just as in the O(3) model considered in this paper. As in the $\sigma$ model, in the spontaneously broken SU(2) gauge theory the period of the periodic instanton increases with energy at low energies, where perturbation theory is applicable [7]. Thus, we conclude that the four-dimensional SU(2)-Higgs gauge theory falls into case (II) for not too strong Higgs self-coupling, and has a sharp crossover at $T_{\rm cr}>T_{-}$ from quantum tunneling to thermal activation in its winding number transition rate.

Apparently, the behavior changes at large $M_H/M_W$, as the model becomes more ''Higgs-like'' and the instanton solutions resemble the scale-invariant SU(2) instantons less and less. At Higgs self-coupling $\lambda\geqslant 8\pi\alpha_W$ (approximately), the SU(2)-Higgs doublet model would appear to lie in case (I). At higher values of $\lambda$ additional static sphaleron solutions bifurcate from the simplest spherically symmetric one, and the semiclassical approximation which requires $\lambda\ll 1$ eventually ceases to be valid [29]. These results have been obtained at zero U(1) mixing angle $\theta_W$. Although sphaleron solutions have been constructed at nonzero $\theta_W$ [30], the negative eigenmode and eigenvalue have not been given in the literature to our knowledge and therefore, we are not yet able to draw any firm quantitative conclusions in the case of nonzero $\theta_W$. However, the behavior of the bosonic sector of the standard model with $\theta_W$ near its physical value is not expected to be very different from the behavior at zero $\theta_W$. In any case, we expect that the physical electroweak theory behaves such as the O(3) model for low to moderate $M_H/M_W$ in case (II) but the situation with the additional Higgs coupling $\lambda$ in $3+1$ dimensions is more complicated and deserving of detailed investigation.

To conclude, the classical solution space of even relatively simple models such as the O(3) model we have studied in this paper appears to be very rich, and the more intricate details of the periodic solutions to four-dimensional spontaneously broken Yang-Mills theories remain to be investigated. Both the analytic and numerical approaches applied here to the O(3) model will extend to the electroweak theory in a straightforward way, and we believe that this program is worth carrying through to completion. In addition to the intrinsic interest of new solutions of the Euler-Lagrange equations of a physical gauge theory, this study, possibly ex-

tended into the complex domain, appears to be the only viable method at our disposal to investigate anomalous baryon-number violation at finite energy in the standard model.

## ACKNOWLEDGMENTS

The authors are grateful to T. Bhattacharya, M. Mattis, M. E. Shaposhnikov, and V. A. Rubakov for helpful discussions. S.H. thanks Eugene Lo of Thinking Machines for advice on the numerics. P.T. wishes to thank D. T. Son, A. Kuznetsov, and S. Yu. Khlebnikov for useful discussions, and the Theoretical Division of LANL for hospitality. S.H. and E.M. acknowledge support from the United States Department of Energy. The work of P.T. was supported in part by the Russian Foundation for Fundamental Research (Grant No. 96-02-17804a) and INTAS (Grant No. INTAS-94-2352). Numerical simulations were performed on the CM-5 at the Advanced Computing Laboratory (ACL), Los Alamos National Laboratory.

[1] G. 't Hooft, Phys. Rev. Lett. **37**, 8 (1976); Phys. Rev. D **14**, 3432 (1976); **18**, 2199(E) (1978).
[2] A. A. Belavin, A. M. Polyakov, A. S. Schwartz, and Y. S. Tyupkin, Phys. Lett. **59B**, 85 (1975).
[3] N. S. Manton, Phys. Rev. D **28**, 2019 (1983); F. R. Klinkhamer and N. S. Manton, *ibid.* **30**, 2212 (1984).
[4] V. A. Kuzmin, V. A. Rubakov, and M. E. Shaposhnikov, Phys. Lett. **155B**, 36 (1985); V. A. Rubakov, Nucl. Phys. **B256**, 509 (1985); Pis'ma Zh. Eksp. Teor. Fiz. **41**, 218 (1985) [JETP Lett. **41**, 266 (1985)].
[5] I. Affleck, Phys. Rev. Lett. **46**, 388 (1981).
[6] B. J. Harrington, Phys. Rev. D **18**, 2982 (1978).
[7] S. Yu. Khlebnikov, V. A. Rubakov, and P. G. Tinyakov, Nucl. Phys. **B367**, 334 (1991).
[8] M. P. Mattis, Phys. Rep. **214**, 159 (1992); E. Mottola, in *Baryon Number Violation at the Electroweak Scale,* edited by L. M. Krauss and S. J. Rey (World Scientific, Singapore, 1992); P. G. Tinyakov, Int. J. Mod. Phys. A **8**, 1823 (1993).
[9] H. Aoyama, H. Goldberg, and Z. Ryzak, Phys. Rev. Lett. **60**, 1902 (1988).
[10] V. A. Rubakov and P. G. Tinyakov, Phys. Lett. B **279**, 165 (1992); P. G. Tinyakov, *ibid.* **284**, 410 (1992); V. A. Rubakov, D. T. Son, and P. G. Tinyakov, *ibid.* **287**, 342 (1992).
[11] J. S. Langer, Ann. Phys. (N.Y.) **41**, 108 (1967); **54**, 258 (1969); S. Coleman, Phys. Rev. D **15**, 2929 (1977); C. Callan and S. Coleman, *ibid.* **16**, 1762 (1977).
[12] A. S. Lapedes and E. Mottola, Nucl. Phys. **B203**, 58 (1982).
[13] E. B. Bogomol'nyi, Phys. Lett. **91B**, 431 (1980).
[14] A. M. Polyakov, Phys. Lett. **59B**, 79 (1975).
[15] A. A. Belavin and A. M. Polyakov, Pis'ma Zh. Eksp. Teor. Fiz. **22**, 245 (1975); A. Perelemov, Physica D **4**, 1 (1981); V. A. Novikov, M. A. Shifman, A. I. Vainshtein, and V. I. Zakharov, Phys. Rep. **116**, 103 (1984).
[16] E. Mottola and A. Wipf, Phys. Rev. D **39**, 588 (1989).
[17] K. Funakubo, S. Otsuki, and F. Toyoda, Prog. Theor. Phys. **83**, 118 (1990).
[18] I. S. Gradshteyn and I. M. Ryzhik, *Table of Integrals, Series, and Products* (Academic, New York, 1980), Eq. 4.295 (7).
[19] Bateman Manuscript Project, *Tables of Integral Transforms,* Vol. I, edited by A. Erdélyi (McGraw-Hill, New York, 1954), Eqs. 1.13 (44) and 2.13 (43).
[20] P. G. Tinyakov, E. Mottola, and S. Habib, in *Quarks '94,* Proceedings of the Eighth International Seminar, Vladimir, Russia, 1994, edited by D. Yu. Grigoriev *et al.* (World Scientific, Singapore, 1995) (hep-ph/9411251).
[21] See, e.g., C. T. Kelly, *Iterative Methods for Linear and Nonlinear Equations* (SIAM, Philadelphia, 1995).
[22] P. Sonneveld, SIAM (Soc. Ind. Appl. Math.) J. Sci. Stat. Comput. **10**, 36 (1989); C. H. Tong, Sandia Technical Report No. SAND91-8240, 1992 (unpublished).
[23] H. A. Van der Vorst, SIAM (Soc. Ind. Appl. Math.) J. Sci. Stat. Comput. **13**, 631 (1992).
[24] W. H. Press, S. A. Teukolsky, W. T. Vettering, and B. R. Flannery, *Numerical Recipes* (Cambridge University Press, Cambridge, England, 1992).
[25] A. A. Abrikosov, Sov. Phys. JETP **5**, 1174 (1957); H. B. Nielsen and P. Olesen, Nucl. Phys. **B14**, 45 (1973).
[26] L. Jacobs and C. Rebbi, Phys. Rev. B **19**, 4486 (1979); J. Baacke and T. Daiber, Phys. Rev. D **51**, 795 (1995).
[27] A. I. Bochkarev and M. E. Shaposhnikov, Mod. Phys. Lett. A **2**, 991 (1987); A. I. Bochkarev and G. G. Tsitsishvili, Phys. Rev. D **40**, 1378 (1989).
[28] V. V. Matveev, Phys. Lett. B **304**, 291 (1993).
[29] L. J. Yaffe, Phys. Rev. D **40**, 3463 (1989).
[30] J. Kunz, B. Kleihaus, and Y. Brihaye, Phys. Rev. D **46**, 3587 (1992); Y. Brihaye and J. Kunz, *ibid.* **50**, 4175 (1994).